**Marine Geology**
May 2022, Volume 447, Pages 106793 (25p.)
https://doi.org/10.1016/j.margeo.2022.106793
https://archimer.ifremer.fr/doc/00762/87388/



# Importance of coarse sedimentation events in the resilience of microtidal back-barrier saltmarshes to sea-level rise

Goslin Jerome [1, 2, *], Bernatchez P. [2], Barnett R.L. [2, 3], Ghaleb B. [4], Béland C. [2], Didier D. [2], Garneau M. [4]

[1] Geo-ocean, IFREMER, 29880 Plouzané, France
[2] Chaire de recherche en géoscience côtière, Université du Québec à Rimouski, Québec-Océan et Centre d'études nordiques, Rimouski, Québec G5L 3A1, Canada
[3] Geography, College of Life and EnvironmeFntal Sciences, University of Exeter, Amory Building, Rennes Drive EX4 4RJ, UK
[4] Chaire de recherche sur la Dynamique des Ecosystèmes Tourbeux et Changements Climatiques, Université du Québec à Montréal, Centre GEOTOP, Montréal, Québec H3C 3P8, Canada

* Corresponding author : Jerome Goslin, email address : jgoslin@ifremer.fr

**Abstract :**

An improved understanding of the resilience capacity of salt-marsh environments, which are recognized as one of the most vulnerable yet valuable coastal morpho-sedimentary systems is important for enhancing resilience to future sea-level rise. The aim of this study is to provide a long-term (multi-centennial) context to the capacity of response of saltmarsh environments to relative sea-level rise by reconstructing the accretion histories of two microtidal back-barrier (one aggradational and one transgressive) saltmarshes in the Bay of Gaspé (Québec, Eastern Canada) over the last centuries. Particular emphasis is put on coarse minerogenic sedimentation and the role it played in the response of the two marshes to relative sea-level changes. To do so, lithostratigraphic, geochronological, and geochemical analyses are carried out on sedimentary cores taken in the back-barrier marsh areas. The accretion histories and the chronology of coarse deposition upon the marshes are reconstructed and yield the following two main results: (1) Coherent yet contrasting records of coarse sedimentation histories are obtained for the two sites, which relate to the distinct configurations and functioning of the fronting barrier systems. The coarse sedimentation time-series of both marshes carry pluri-decadal periodicities typical of atmospheric and intra-oceanic modes of variability, as well as periodicities of 18.0 to 18.5 years, which are interpreted as the expressions of the influence of the 18.6-year nodal tidal cycle. (2) We observe intra- and inter-site variations in the accretionary behavior of the two systems as well as in their respective histories of coarse minerogenic deposition. We show that coarse sedimentation at the surface of the two marshes has been crucial for maintaining accretion rates both in minerogenic and organogenic environments, and thus for allowing saltmarshes to build a resilience capacity in a regime of relative sea-level rise.

**Highlights**

► Last centuries records of coarse sedimentary deposition are reconstructed from two saltmarshes. ► Large-scale climate dynamics and the nodal tidal cycle control coarse minerogenic sedimentation. ► Periods of enhanced minerogenic deposition are driven by episodic coarse sediment inputs. ► Saltmarshes pseudo-equilibrium with RSL partly depends on episodic coarse inputs. ► Capacity of coarse sedimentary material to reach back-barrier marshes should be promoted.

**Keywords** : Sandy barrier, Saltmarshes, Sea-level, Accretion rates, Resilience, Washover, Storminess

## 1.Introduction

Frequencies of extreme water levels and the inundation of low-lying coastal areas will increase due to relative sea-level rise (RSLR), whether or not storm activity intensifies (Clemmensen et al., 2016; FitzGerald et al., 2008; Williams, 2013). The risk to human activities and infrastructure from extreme water level events and coastal inundation is considerable (Cazenave and Cozannet, 2014; Hinkel *et al.*, 2014) and so is the threat pending on the sustainability of coastal lowlands landforms and associated ecosystems such as saltmarshes. These fulfill several important roles in coastal resilience such as storm surge attenuation along open coasts exposed to large swells (Temmerman *et al.*, 2012; Leonardi *et al.*, 2018), barrier/back-barrier structural stabilization (Schuerch et al., 2018a; Walters et al., 2014), global climate change mitigation (e.g. blue carbon sequestration capability ,Mcleod *et al.*, 2011; Pendleton *et al.*, 2012), ecosystem services and ecological sustainability (nursing and migratory habitats, Cattrijsse & Hampel, 2006; Barbier *et al.*, 2011;). However, the persistence of these systems under RSLR and reinforcement of storminess fostered by ongoing climate change is in question (Crosby *et al.*, 2016; Sanju *et al.*, 2017; Schuerch *et al.*, 2018b). The persistence of saltmarshes is largely dependent on accretion rates, as determined by sediment and nutrient flux and *in situ* biomass production (e.g., Gunnell *et al.*, 2013). By modifying the sediment supply and budget, storms and associated submersion events are known to negatively affect the resilience capacity of back-barrier saltmarshes (Leonardi *et al.*, 2018). Conversely, storm activity is also known to contribute to marsh surface accretion rates by increasing suspended sediment delivery (e.g. Bartholdy *et al.*, 2004; Schuerch *et al.*, 2012) and the deposition of suspended sediment farther into marsh interiors (e.g. Schuerch *et al.*, 2018a). These contrasting perspectives both support the notion that it is not possible to accurately predict saltmarsh resilience to future sea-level rise without reconciling storm-driven sediment budget variability and associated feedbacks between inundation,

sediment transport and deposition and vegetation dynamics (Leonardi *et al.*, 2018; Wiberg *et al.*, 2020).

The aim of this contribution, therefore, is two-fold: 1) to reconstruct records of past coarse sedimentation in the two studied saltmarshes over the last centuries and 2) to gain insights on the role coarse sedimentary deposits played in the century-scale adaptation of back-barrier marshes to RSLR, with a particular interest in studying the differences between transgressive and aggrading systems. To accomplish this, we investigated the sedimentary archives of two back-barrier salt marshes in the Bay of Gaspé (Gulf of St. Lawrence, Eastern Canada) selected as representing typical aggrading and transgressive barrier-marsh systems of microtidal areas (Bernatchez *et al.*, 2013). Sedimentological and geochemical analyses were carried out on sediment cores taken from the two marshes and used to derive a chronology of coarse sediments deposition (referring hereafter to sediments coarser than modal fair-weather marsh sedimentation) and back-barrier marsh accretion over the past 400 years. Coarse sedimentary events were traced back within a high-resolution geochronological framework while grain-size distributions were statistically analyzed to document periodicities in marsh coarse sedimentation. The results we obtained allow us to address the following questions: 1) What drives coarse sediment deposition event variability over multi-centennial scales? 2) How do marsh accretion rates respond to coarse sedimentary inputs and centennial-scale RSLR, and what are the implications for the resilience capacity of salt marshes into the future? By comparing the behaviors of two aggrading vs. transgressive marshes subjected to exact similar forcing, we believe our results carry implications for a better understanding and management of barrier systems established in similar microtidal settings worldwide.

## 2. Regional setting

The Bay of Gaspé is a 36 km long flooded glacial trough with a northwest-southeast orientation at the eastern extent of the Gaspésie Peninsula (Québec, Eastern Canada) (Fig.1-I), carved through the Gaspé Sandstone Formation (Allard & Tremblay, 1981). The region belongs to the Gaspé Belt, a

geological ensemble juxtaposing synclinal formations dating from the Late Ordovician / Early Silurian to the Late- to Mid-Devonian (Saint-Laurent *et al.*, 2004). The Bay of Gaspé shares its Holocene isostatic history with the Maritimes provinces (Koohzare *et al.*, 2008, Bernatchez *et al.*, 2013) and has experienced subsidence since the Early Holocene (Shaw *et al.*, 2006; Vacchi *et al.*, 2018). The closest high-resolution relative sea-level (RSL) reconstruction is from the Chaleurs Bay (Barnett *et al.*, 2019), approximately 120 km to the southwest of the study region (Fig.1-I). Following deglaciation, RSL dropped rapidly to reach a low-stand at -20 to -30m below present-day sea level between ca. 10500 and 9500 cal. yrs B.P. (Bernatchez *et al.*, 2013). Following the low-stand, RSL rose continuously until present by >2 m during the past two millennia (Barnett *et al.*, 2019). Over the past ca. 500 years, RSL rose at a mean rate of 0.93 ± 1.25 mm $yr^{-1}$. An acceleration in the rate of RSL rise occurred shortly after the Little Ice Age (ca. 1600 CE), and more recent episodic accelerations have been observed at ca. 1850, 1950 and 1990 CE, possibly relating to ocean mass redistribution during phases of climate modes, as well as ocean mass changes (e.g. from polar ice-sheet mass fluxes) (Barnett *et al.*, 2019).

**3. Study sites**

3.1. Sites physiography and formation

The study sites are two back-barrier salt marshes located on either shoreline of the inner Bay of Gaspé (Fig. 1-II) The rationale for site selection was that: 1) while being exposed to equivalent oceanographic forcing, the short-term evolution of the two systems as well as their sensitivity and resilience to storm events differed (Bernatchez *et al.*, 2013), and 2) the two sites represent differing accumulation regimes - aggradational for one (Penouille, north shore of the bay) and retrogradational (also termed transgressive) for the other (Sandy Beach, south shore). Penouille is a lagoonal salt marsh located on the northern shore of the bay. It formed behind a southwest-northeast orientated spit system connected to the coastline by a narrow ridge (isthmus) (Allard & Tremblay, 1981; Fox *et al.*, 1995) (Fig. 1-III). The spit system developed upon a Holocene deltaic wedge (Fox *et al.*, 1995) ~900 to 800 cal. yrs B.P. (Bernatchez *et al.*, 2013) before prograding

eastward with more than 40 stacked beach-ridges that started forming ~600 cal. yrs B.P. The system follows an aggrading evolution and has remained approximately stable since at least 1765 C.E. Sandy Beach is situated on the southern shore of the bay (Fig.1-II) and consists of a double-spit system, which encloses the salt-marsh site (Fig. 1-IV). Similarly to Penouille, Sandy Beach also sits upon a submerged deltaic plain, attested to by the coarse grey sand basal facies on which the two marsh successions encroached upon (Gibeault *et al.*, 2016 and this study). Dates previously obtained at the base of Sandy Beach organic formations suggest that marsh sedimentation began ca. 724 cal. yrs B.P. (Bernatchez *et al.*, 2013). In Penouille, the spit system is fed by longshore sediment transport containing sandstone cliff material from the east of the site. The composition of modern beach sand is dominated by quartz material (85%), with fragments of volcanic (5 %), clayey-shale (4 %) and mafic rocks (3 %) (CSSA Consultants, 1992). Marsh sediments show a bimodal grain-size distribution with two clear sandy and silty-clayey pools of material (Gibeault *et al.*, 2016). At Sandy Beach, the longshore transport, alongside nearshore bar dynamics, is also the main provider of sediments to the system, bringing eroded material from the Gaspé Sandstone Formation to the spit. Due to a drastic reduction in the sediment supply by the latter, the system is considered to be in serious sedimentary deficit.

3.2 Local hydrodynamic setting

The bay of Gaspé has a microtidal regime (max. spring tidal range: 1.7 m) and follows a semi-diurnal cycle. Powerful swells fed by a ~400 km fetch can enter the bay during storms from the north-eastern to the south-eastern sectors. For the 1980-2017 period, the outputs of the WaveWatch III model at two offshore grid points located at the entrance of the bay (point “VB1” on fig.1-II, 93 m water depth) and in the inside (point “VB2” on fig.1-II, 42 m water depth) show a strong attenuation of the wave height in the bay (performance of the WWIII model in the study region attested by Bandet *et al.*, 2020 and Didier *et al.*, 2019 ). Average significant wave height (Hs) drops from 0.40 m to 0.13 m between points VB1 and VB2; whereas 99$^{th}$ percentile Hs drops from 2.83 m

to 1.15 m. Results of instrumental measurements (AWAC profilers, noted AW1 and AW2 on figs. 1-II and 1-III) made in the foreshore and nearshore domains at Penouille during autumn 2010 and 2011 confirmed this attenuation of the wave towards the inner part of the bay, waves height being observed to dampen by 40 to 60 % between AW1 and AW2 (Bernatchez *et al.*, 2013). This attenuation of wave-energy is due to the action of the subtidal bars that extensively cover the nearshore domain of the two study sites, even if this influence rapidly declines as water-level increases (Bernatchez *et al.*, 2013). Despite such low wave amplitudes, which are typical of fetch-limited coasts, joint occurrences of high-water levels and short waves (i.e. peak period, $T_p$ < 5 s) in the nearby Chaleur Bay have been associated with intense overwash events and inland sediment transport, producing extensive washover lobes (Didier *et al.*, 2019). More rarely, westerly winds can also raise small waves in the inner part of the bay, that may enter the lagoon of the Penouille site.

## 4. Material and methods

### 4.1. Recent evolution of salt marsh - spit systems

We used recent shoreline dynamics of the Penouille and Sandy Beach spits to highlight the functioning differences of the two sites (fig. 2). Data used for this purpose was obtained in a previous study of Bernatchez *et al.* (2013) for a report produced for the Canadian natural parks authorities. At each site, shorelines were georeferenced and digitized over the 1948-2010 periods from aerial photographs using the limit of dense herbaceous vegetation (maximum high-water level) or at the top of microcliffs as benchmarks. Shoreline migration rates were then calculated at 50 m horizontal intervals using the DSAS plugin in ArcGIS© software (Thieler *et al.*, 2009). The areas of the saltmarshes, beach and spit domains were mapped for Penouille on the 1963-2008 period and for Sandy Beach over the 1948-2008 period using the oldest and most recent aerial photographs available at each site and georeferenced in the ArcGIS© software. Marsh areas were computed using polygons following the outer marsh edges drawn on the aerial photographs.

### 4.2. Reconstruction of past submersion events

4.2.1. Surveying and coring

Fieldwork was carried out in August 2018. Reconnaissance cores were first obtained along cross-shore and longshore transects (Figs. 1-III and 1-IV) using a narrow-gauge gouge auger (green dots on figs. 1-III and 1-IV). These cores were used to describe sedimentary facies successions and to establish stratigraphic frameworks for each site. For each site, three analytical cores were then sampled from locations optimizing the recovery of coarse sedimentary deposits (red stars on figs. 1-III and 1-IV). Analytical cores were retrieved using a 1 meter long 50 mm gauge open gouge-auger, which ensured sediment compaction was kept minimal during recovery. Core locations were surveyed with a Trimble RTK DGPS station tied to the Canadian Spatial Reference System North American Datum 1983 using locally available benchmarks. Elevation data are based on the Canadian Geodetic Vertical Datum of 1928 (CGVD28) following a correction from the geoid model HT2.0. At Penouille, core PEN-ST3-1was taken in the high marsh domain ~20m behind the crest of the Penouille spit (Fig. 1-III). Cores PEN-ST3-2 and PEN-ST3-3 were retrieved further onshore along the cross-shore transect 3 (Fig. 1-III), ~10 and 20m north of PEN-ST3-1. In Sandy Beach, analytical cores were retrieved at the proximal end of the cross-shore transect SB STM (Fig. 1-IV). Core SB-STM-1 was taken juts behind the barrier from the surface of a recent washover deposit (Fig. 1-IV), while cores SB-STM-2 and SB-STM-3 were taken 31 and 67m west towards the inner back-barrier marsh domain (Fig.1-IV).

4.2.2. Core analyses

Each analytical core was cleaned and photographed on site, then wrapped in plastic and stored horizontally in PVC guttering. In the laboratory cores were mounted within transparent PVC for analysis in a Geotek © multi-sensor core logger (MSCL) at the Institut des Sciences de la Mer de Rimouski (ISMER, St-Onge *et al.*, 2007). Whole cores were analyzed by the MSCL at 1 cm increments for gamma density and magnetic susceptibility using a Barrington MS2E1 point-sensor. Cores were split lengthwise and half-cores were analyzed again on the ITRAX module at 0.5 cm to 1 cm steps for high-resolution imaging, digital X-ray imaging (XCT) and X-Ray fluorescence (XRF). Out of 36 major

and trace elements, only the elements showing substantial variations downcore were kept for further statistical analyses (Ti, Mn, Fe, Zn, Rb, Sr, Y, Zr, Al, Si, S, K, Ca). Reference cores were sampled at 1 cm intervals to obtain Loss-On-Ignition (LOI) and grain-size analytics. Samples were dried at 150 °C overnight to measure water content and then at 550 °C for 4.5 hours to measure the LOI. Grain-size analyses were performed on a Beckman-Coulter LS-13320 using the post-LOI mineral remains washed from the organic ashes. Samples were soaked and agitated for 3 hours in a solution of sodium hexametaphosphate ($NaPO_3$) at 20 $g.L^{-1}$ to ensure adequate deflocculating before measurement. Results were finally summarized using Gradistat 8.0 (Blott and Pye, 2001).

4.2.3. Chronology

Reference cores PEN-ST3-1 and SB-STM-1 underwent AMS radiocarbon dating at Keck carbon cycle AMS facility (University of California, USA) on manually picked and identified plant macro-remains (Table 1). When sufficient amount of material was available, samples were pre-treated at the Laboratoire de Radiochronologie (Centre d'études Nordiques (CEN), Université Laval, Québec city, Canada) following a HCl-NaOH-HCl sequence. Ages were calibrated against the IntCal13 calibration curve (Reimer *et al.*, 2013) and are reported at the 2σ (95.4 %) confidence level. The top of each reference core was also sampled for $^{210}Pb$ radionuclide analyses at 1 to 1.5 cm steps down to the 18 cm depth (Table 2). Sampling was carried out using a ceramic knife and Teflon tools to rule out the eventuality of pollution by lead-bearing metal. Samples were prepared following Not *et al.* (2008). Sediment was dispersed with milli-Q deionized water and every root, rootlet and plant macro-remains were removed to remove the influence of $^{210}Pb$ free material on the total weight of the sample. Samples were then fully dried at max. 60°C and ground within an agate mortar. Samples were spiked with $^{209}Po$, treated using a $HCl/HNO_3$-$/HF/H_20_2$ sequence (Baskaran and Naidu, 1995). Residues were mounted onto a silver disc and the $^{209}Po$ and $^{210}Po$ activity (used as a proxy for supported $^{210}Pb$) was measured using an alpha spectrometer EGG and ORTEC type 576A at Géotop (Université du Québec à Montréal, Canada). Uncertainties were estimated as 1-σ standard deviation for counting statistics (Table 2). Finally, the results were normalized by the proportion of fines (< 63

µm) to compensate the effect of grain-size on the fixation of $^{210}$Pb in the sediments (Arias-Ortiz *et al.*, 2018). As studied cores were subjected to irregular inputs of tidally-derived material and by the deposition of sandy material during storm-surges, we used the "constant rate of supply" model (Appleby and Oldfield, 1978) especially suitable for environments concerned by irregular changes in the accretion rates (Ghaleb, 2009). Finally, a correction was applied using downcore gamma density measurements to account for the non-linearity of accumulation rates over time.

4.2.4. Statistical analyses

*(i) Identification of coarse sedimentary events*

Reference cores PEN-ST3-1 and SB-STM-1 were analysed for the intra-class deviation of grain-size data on the organic marsh sections. This allowed to separate the grain-size classes characterized by a continuous presence alongcore from those showing higher variability, and thus to decipher between background sedimentation and punctual coarser sedimentation events (e.g. Sabatier *et al.*, 2012). All fraction coarser than background minerogenic sedimentation will be referred to in the text as "coarse sedimentation", regardless of their effective coarseness on traditional grain-size charts. In order to get a geochemical characterization of the coarse sedimentation events and to reach a more precise localization these latter downcore, we performed Principal Component Analyses (PCA) on centered and reduced (Z-score) major and trace elements data normalized by Al (PEN-ST3-1 core) or Ti (SB-STM-1 core), $D_{50}$ and $D_{90}$ grain-size data and LOI data using the "FactomineR" (Lê *et al.*, 2008) package in R software (R core team, 2020). The "missMDA" package was used to allow for missing data (such as produced by the occurrence of below detection values for the Al and Ti elements used for normalization).

*(ii) Spectral analyses of past submersion time-series*

Reference cores PEN-ST3-1 and SB-STM-1 $D_{90}$ grain-size time-series were subjected to spectral analyses to look for periodicities in the occurrence of coarse sedimentation events. The analyses used the Multi-Taper spectrum (MTM; Thomson, 1990) and the wavelet transform (Evolutive

Harmonic Analyses, EHA (Kodama & Hinnov, 2014) functions of the R software (R Core Team, 2020) Astrochron package (Meyers *et al.*, 2014). Prior to the analyses, $D_{90}$ grain-size time-series were re-interpolated at a 5-yr step and detrended using a 1/1 LOWESS smoothing (Locally weighted scatterplot smoothing, Cleveland, 1979), so as to avoid long-term trends in grain-size data (e.g. a linear increase of washover deposits grain-size linked to a diminishing distance to the coastline) that might obscure the identification of coarse sedimentation events. MTM and EHA analyses were performed using a padding factor of 10 and window sizes comprised between 180 and 600 years. Confidence levels were estimated using a red noise fit (ML96; Mann and Lees, 1996).

## 5. Results and discussion

### 5.1. Recent evolution of the two spit-marsh systems

At Penouille, the position of the spit shoreline remained approximately stable over the 1948-2010 period (Fig. 2-A). The system experienced a positive migration at a rate of 0.07 m.yr$^{-1}$, in line with the aggradationnal functioning of the system (Fig. 2-A). The beach-spit system at Penouille increased in area by 3.5 %, whereas the marsh area reduced slightly by -1.3 % (Table 3). In contrast, the shoreline at Sandy Beach retreated at a mean rate of -1.07 m. yr$^{-1}$ over the 1948-2010 period (Fig. 2-B) and a net onshore migration of the system was observed. The distal end of the spit retreated by 620 m between 1948 and 2010. The surface area of the Sandy Beach beach-spit reduced by 55.33 % over the 1948-2010 period, while 24.31 % of the marsh area was lost (Table 3). The state of disequilibrium of the Sandy Beach spit system, as demonstrated by these results, is thought to be due to a reduction in sediment delivery to the system by longshore transport, as well as to the retreat of the barrier during storm events reducing the area of the marsh.

### 5.2. Analysis of Penouille marsh sedimentary archives

#### 5.2.1. Description of the sediment cores

Core PEN-ST3-1 sampled 55.5 cm of marsh sediments before reaching underlying coarse sand deposits (Unit 1) (Fig. 3-A). Above, the organic marsh succession is then characterized by a bi-modal

sedimentation consisting of medium sand material with an organic silty component (Fig.3-D and 3-E; modes respectively centered around 69 µm and 179µm; mean grain-size 110 µm, mean LOI of 18.9 ± 4.8 %). From 55cm to ~32cm depth, sedimentation is made silty sand deposits (Unit 2, mean grain-size 65.7 ± 32 µm, mean LOI of 18.86 ± 4.5µm; Fig.3-C to E). The whole unit is marked by a prominent presence of medium to coarse sand (Fig. 3-D). A marked change occurs at 32cm deep, the mean grain size falling from >140µm to 70µm (Fig. 3-D and E). This materializes the onset of unit 3 (D50 47.8± 4.5µm). From 13cm deep, the sharp increase in organic content (to values of 40 ± 17%; Fig. 3-E) transforms the sediment into gyttja, materializing the onset of high salt marsh deposit conditions (Unit IV). The highest grain-size intra-class standard deviations are observed for the 213-450 µm and the 450-1300 µm classes (Fig. 3-D). These latter show very irregular and pulsative frequency distributions downcore (Fig. 3-D to F) materializing pulses of medium to coarse sand inputs superimposed on the background sedimentation (Fig. 3-D). These sand-enriched beds show up as rather diffuse pluri-centimetric beds at the base of the core (30 to 55cm depth) and as better-defined sub-centimetric beds above 30 cm depth. In the bottom part of the core, the identification of these beds is blurred by the presence of the sandy embedding matrix (Fig. 3-A, B and D). Beds are either sub-horizontal or display steep downlap-like landwards dipping of ~20 to ~30°. In-depth description of the sedimentary characteristics of these layers follow in section 5.2.4.

Core PEN-ST3-2 is 75 cm long. It is characterized at its base (75-50 cm depth) by coarse grey sand deposits comparable to the one of core PEN-ST3-1 unit 1 (Fig. 4-I-B). It then progressively fines upwards (unit 1') and gains organic matter to resemble an organic silty sand at the 30 cm depth (unit 2). It then turns into an organic silt deposit at 33 cm depth (unit 3) and later into a gyttja high marsh deposit (unit 4) from ~15cm deep (Fig. 4-I-B). Above the 30 cm depth, the succession is marked by centimetric to pluri-centimetric well-individualized sand beds, clearly showing up both visually as well as on the X-Ray image (Fig. 4-I-B). Core PEN-ST3-3 is 80 cm long (Fig. 4-I-C). Coarse grey sand (unit 1) is again observed at the base (80 to~60cm depth) (Fig.4-I-C). Succession is then very similar to PEN-ST3-2, the sediments progressively gaining organics to the top. A densely rooted gyttja is found

from 30cm deep up to the core top. A diffuse presence of coarse sand grains is noted throughout the entire marsh-type sequence but a well-defined sand bed is only notable at the top of the core (6-10cm depth; Fig. 4-I-C).

**5.2.2 Age model**

The age-depth model of core PEN-ST3-1 was built on six radiocarbon dates and sixteen $^{210}Pb$ measurements (Fig. 5-A, tables 1 and 2). A $^{14}C$ date of seeds sampled at the base of the marsh stratigraphy (55.5 ± 0.5 cm depth) yielded a calibrated age of 478-318 cal. yrs B.P. (median age 381 cal. yrs B.P.) (Fig. 5-A; Table 1). This establishes the onset of Penozhic marsh formation around 1569 C.E., in accordance with an emersion phase previously identified for the same period from $\delta^{13}C$ measurements performed on an equivalent succession (Bernatchez *et al.*, 2013) and by the previous ages obtained on the same site by Gibeault *et al.* (2016). This emersion phase followed a transgressive-erosive period dating back to 645-417 yrs cal. B.P., which is considered to have favored the establishment of the second generation of Holocene salt marshes in the region (Bernatchez *et al.*, 2013). Once established, marsh sedimentation occurred at a constant pace until 13 cm in the core (median age 1885 C.E.), where a decrease in sedimentation rates is observed (Fig. 5-A), reflecting the onset of high-marsh conditions at the location of the coring site, which is further corroborated by changes in sedimentary facies and LOI observed at the same level (Fig. 3).

**5.2.3. Major and trace elements**

The PCA performed on the sedimentological and geochemical variables of core PEN-ST3-1 (marsh succession only; 0-54 cm deep) reveal clear tendencies within the marsh stratigraphy (Fig. 4-II). Dimension 1 summarizes 44.23 % of the variability and portrays the opposition between organic sedimentation within the marsh (characterized by high LOI values) and periods of minerogenic enrichment (characterized by elemental enrichment within the core) (Fig. 4-II). Dimension 2 summarizes 23 % of the observations and describes a strong anticorrelation between: (i) enrichments in Ca, Sr, Zn and Rb which, associated with high LOI values, characterize the modal salt marsh fine

sedimentation and (ii) enrichments in Ti, Si, Zr, Y, K and S which are associated with increases in the $D_{50}$ and $D_{90}$ grain-size values, thus describing periods of coarser sand sedimentation in the marsh (Fig. 4-II). These prompted us to use downcore relative negative excursions of PCA dimension 2 as an indicator of coarse sedimentary events within PEN-ST3-1, supplementary to grain-size information. PCAs performed on cores PEN-ST3-2 and PEN-ST3-3 displayed very similar relationships between the geochemical variables (Fig. 4-II). In absence of grain-size analyses made on these two cores, this allowed us to use negative excursions of PCA dim. 2 and positive peaks in the Si/Rb ratio as proxies of grain-size for the latter cores (Fig. 4-I).

**5.2.4. Coarse sedimentary layers: identification and sedimentary characteristics**

We identified a total of 17 coarse sedimentary events in core PEN-ST3-1 (Table 4). For most of the layers identified within core PEN-ST3-1, very clear correspondences could be drawn within cores PEN-ST3-2 and ST3-3, demonstrating the rather large spatial extent of the coarse sedimentary beds across the marsh. The coarse beds display a constant pluri-modal grain-size distribution (Fig. 6-A), showing these to originate from a mixture of different sources. The sand component of these layers is characterized by a bi-modal distribution (Fig. 6-A), centered around 1.6-2phi (280-300 µm) and 0.4-0.6phi (580-650 µm peaks), blend together with the silt to fine sand background sedimentation (Fig. 6-A). Inclusive sorting vs. inclusive mean scatterplot (Fig. 6-B) clearly distinguishes coarse layers from the modal background marsh sedimentation, the former being much better sorted. Skewness vs. D50 scatterplot shows only little difference between coarse layers and background marsh sedimentation, the formers being in general only slightly more negatively skewed (Fig. 6-B). Peak-to-peak correspondences could be drawn with rather good confidence between coarse events identified in core PENST3-1 and peaks in the Si/Rb ratio and negative excursion of PCA dimension 2 of cores PEN-ST3-2 and PEN-ST3-3 (Fig. 4-I). Sand beds are especially well-defined in core PEN-ST3-2, even better individualized and defined than in core PEN-ST3-1 (Fig. 4-I-B). On the contrary, even if still identifiable in the geochemical proxies, coarse sedimentary layers are found with a much reduced strength in core PEN-ST3-3 (Fig. 4-I-C).

### 5.3. Analysis of Sandy Beach marsh sedimentary archives

#### 5.3.1. Description of the sediment cores

Core SB-STM-1 retrieved 73 cm of sediments, from which only 60 were analyzed (Fig. 7). Between 60 and 38 cm deep lays a very constant low organic (LOI of 10.2 5 ± 3.3 %) medium to coarse grey sand deposit (D50 = 214 ± 97 µm) with a light silty component (Unit 1, Fig. 7-A to E). From 38 cm deep and until 30 cm, the sedimentary facies evolves into a slightly more organic and much more layered sand facies (unit 2, Fig. 7A to E). A sharp change occurs at 30-cm deep (Fig. 7D and E). Background sedimentation then transitions into a low organic (LOI 13.9 ± 0.8 %) fine silty deposits of median grain-size 47 ± 53 µm (Unit 3), revealing the onset of tidal flat to low-marsh deposit conditions at the site. From 24cm deep, the organic content increases considerably towards the core top (unit 4, reaching up to 59 % in the uppermost 5 cm) while the silty sedimentation stays constant (Fig.7-D), materializing the progressive evolution towards mid- to high-marsh conditions. The 213-863 µm class (peak at 493 µm) is the grain-size class that displays the highest intra-class standard deviation across the marsh succession retrieved by core SB-STM-1 (Fig. 7-D), materializing the presence of pulses of medium to coarse sand inputs punctually interrupting the modal marsh sedimentation (Fig. 7-D to F). These sand layers take the form of horizontal to slightly dipping medium to coarse sand beds of 1 to 4 cm thicknesses (Fig. 7A and B), and are marked by peaks in the Ti, Si and Zr contents (Fig. 8-).

Core SB-STM-2 retrieved 55 cm of sediments (Fig. 8-I-B). The first 30 cm (25.5 to 55 cm deep) are composed of slightly organic sand material very similar to the one of core SB-STM-1 unit 1 (Fig. 8-I-B). This layer fines upwards and gains organic content, turning into a root-rich silty sand to gyttja marsh deposit around 25 cm deep (unit 3). Unit 2 identified in SB-STM-1 could not be recognized (Fig. 8-I-B). From 20 cm and upwards, the sedimentation turns into a gyttja-like deposit (unit 4), only interrupted by punctual enrichments in sand content associated with positive excursions of the Si and Zr contents

(Fig. 8-I-B). A layer particularly rich in coarse sand grain is noted between 7 and 12 cm deep (Fig. 8-I-B). Core SB-STM-3 sampled 52 cm of sediments (Fig. 8-I-C). Basal 10 to 15 cm are composed of basal coarse grey sand (unit 1). From around 35 cm deep, sedimentation gains silt material (unit 2; Fig. 8-I-C). A sharp increase in organic content and roots presence is observed from 23 cm deep, from where sedimentation displays gyttja-like facies (unit 3), really established from 18 cm deep (Fig. 8-I). The top 15 cm of the core are marked by the presence of well-individualized horizontal event beds, popping-up on the X-rays, and associated with clear peaks in Zr and Si (Fig. 8-I-C).

**5.3.2 Age model**

The chronological framework built for core SB-STM-1 relies on 5 AMS $^{14}$C dates (Table 2; Fig. 9-A) and 15 $^{210}$Pb measurements (Table 2; Fig. 9-B). The deepest radiocarbon date was obtained at 57 ± 1 cm and yielded a median age of 1360 yrs cal. B.P. (1392-1319 yrs cal. B.P.; Table 1). A couple of $^{14}$C dates performed at 38.5 ± 0.5 cm and 37.5 ± 0.5 cm deep delivered respective ages of 1123 yrs cal. B.P. (1178-1064 yrs cal. B.P.) and 546 yrs cal. B.P. (628-522 yrs cal. B.P.) (Table 1) hence confirming the existence of a sedimentary hiatus at 38 cm deep (Fig. 9-A). Sedimentation started again above the hiatus at 714 yrs cal. B.P. (951-1431 yrs cal. B.P., 1236 C.E.). Organic marsh sedimentation settled around 1700 C.E. (250 yrs cal. B.P.), in accordance with the sedimentation model previously established by Bernatchez *et al.* (2013).

**5.3.3. Major and trace elements**

The PCA performed on the marsh succession of core SB-STM-1 (0-30 cm deep) shows a clear separation between modal sedimentation and event and sandy layers (Fig. 8-II). PCA dimension 1 summarizes 57.48 % of the observations and displays an opposition between a strong positive loading characterized by high content in Si, Nb, Ti, Zr, S, K, Ca, Sr, Rb, Fe and Zn, describer of a minerogenic environment, and a negative loading pulled by Mn and LOI, characterizing organic deposition (Fig. 8-II). Dimension 2 is a more useful describer for the purpose of this study. It

summarizes 15.33 % of the data and opposes levels of fine sedimentation rich in Zn, Fe, Rb, Sr, and Ca to layers of coarser sedimentation characterized by enrichments in Si, Nb, Ti, Zr (and to a lesser extent S and K) and peaks in $D_{50}$ and $D_{90}$ grain-size (Fig. 8-II). Hence, negative excursions of PCA dim. 2 were further used as a proxy for coarse sedimentation downcore core SB-STM-1. Similar relationships between the elements were observed for the SB-STM-2 and SB-STM-3 cores (Fig. 8-II). Considering this, we used negative excursions of PCA dimension 2 and positive excursions of the Si/Rb ratio to draw correspondences between events identified in reference core SB-STM-1 and cores SB-STM-2 and SB-STM-3 (Fig. 8-I). Clear correspondences could be made, showing the rather large lateral extension of the coarse sedimentary events identified in core SB-STM-1 (Fig. 8-I).

**5.3.4. Coarse sedimentary layers: identification and sedimentary characteristics.**

We identified nine coarse sedimentary levels in the Sandy Beach marsh succession, whose depth-in-core and reconstructed ages are listed in table 4. These events layers have a sedimentary signature remarkably different than background marsh sediments (Fig. 10-A). All event layers are characterized by a much coarser mean grain size, with a dominating mode peaking around 1-2 phi (full range from 0 to 3 phi) (Fig. 10-A). This grain-size signature is very similar the one obtained for 14 samples taken across the surface of a modern washover deposit close to the coring site (Fig. 10-A). Events layers also display with much higher skewness values (0.3-0.9 phi; Fig.10-B) than those displayed by modal marsh sediments (-0.1 to 0.3 phi; Fig. 10-B). They as well appear generally much better sorted, even if some dispersion is to be noted (Fig. 10-B). Using peak-to-peak correspondences of the Si/Rb ratio and PCA dim. 2 curves, most of the layers identified within core SB-STM-1 can be followed landwards within core SB-STM-2 and SB-STM-3 (Fig. 8-I). On the PCA biplots, Zr progressively slides from the pool of variables associated with coarse-grained sedimentation to the one associated with fine sediments as we progress landwards (Fig. 8-II).

**5.4. Spectral analyses of grain-size time series**

Spectral analyses of the coarse-sedimentation event reconstructions identified several periodicities at both Penouille and Sandy Beach (Fig. 11). For Penouille, MTM and EHA analyses identified three dominant periodicities (130, 18.5 and 12.5 yrs) at the 90 % confidence level within core PENST3-1 grain-size time-series (Fig. 11-A). The periodicity centred around the 130-yr wavelength is rather discontinuous and evolves into a 90-yr period from 1900 C.E (Fig. 11-A-IV). The 18.5-yr period exceeds the 99 % confidence level and remains stationary throughout the majority of the record (Fig. 11-A-III and IV). The output of a band-pass filter centred on an 18.6-yr period shows strong coherence with the $D_{90}$ grain-size time series at Penouille (Fig. 11A-II), raising trust in the fact that the occurrence of coarse-grained sedimentation on the marsh of Penouille obeyed a control factor varying at or around this periodicity. Finally, the 12.5 yr periodicity is only patchy and present during 60-yr over the 1740-1800 C.E. period (Fig. 11-A-IV). In slight contrast, spectral analysis of the Sandy Beach coarse-sedimentation time-series reveals three dominant periodicities (above 90 % confidence levels), centred around the 163, 47-55, and 18-yr wavelengths (Fig. 11-B-III). The 163-yr period seems to blend together 100 to 200-yrs periods. It is especially prominent between 1580 and 1800 C.E. before vanishing towards younger ages (Fig. 11-B-IV). The ~50-yr periodicity (45 to 60-yrs range) establishes itself from this precise period and remains stationary across the 20$^{th}$ century before disappearing in the last decades (Fig. 11-B-IV). Finally, a 18-yr periodicity is also evidenced by the MTM and EHA analyses, showing up with a very low-power still a fair reliability (90 % confidence level) from around 1800 C.E., i.e. when temporal resolution of the record increases (Fig. 11-B-III and IV). The 18-yr band pass filter output nonetheless shows great coherence with the $D_{90}$ grain-size time series at this site after 1900 C.E., but not before, potentially as a result of lower temporal resolution (Fig. 11-B-II).

## 6. Discussion

### 6.1. Origins of the coarse sedimentary layers

6.1.1. Penouille marsh

In Penouille, several hypotheses can be put forward to explain the presence of layers of sand within the back-barrier marsh sedimentary successions. The first hypothesis is that these were deposited by overwash dynamics during onshore storms. Arguments in favor of this origin are several: (i) The events layers share common sedimentary characteristics (especially a much better sorting than modal marsh sediments) with the sand layers whose ages correspond to storm wave events listed in the Forillon Canadian Parks archives as having massively impacted the site (such as the 6-7 cm depth layer which was most likely deposited by the storms of December, 1968 for which washovers were witnessed to have deposited on the Penouille back-barrier marsh); (ii) The bi-modal character of the sand fraction of the "coarse" layers echoes the bi-modal grain-size distribution of the sand from the foreshore to beach domains (Fig. 6; Bernatchez *et al.*, 2013), thus advocating for an offshore origin of the sand found within the cores and (iii) Coarse sedimentary layers can be traced across the marsh with a tendency to vanish landwards (Fig. 4). A counter argument is the fact that grain-size distribution of the event layers is rather evenly spread over sand and fine-grained fractions (Fig. 6), while the traditional vision of overwashes entering back-barrier marsh areas is that these cause the deposition of sand sheetwashes over the back-barrier marshes (e.g. Phantuwongraj *et al.*, 2013). Nonetheless, it is without considering the potentiality that overwashes could have occurred in an overwash rather than inundation regime (Morton and Sallenger, 2003), where water fluxes would have been high enough to overtop the barrier crest and transport sand in suspension to the back-barrier area but not sufficiently powerful to carry massive amounts of sand over the marshes (e.g. Williams, 2012). Such process would also explain the absence of clear erosive contact at the base of most of the coarse sedimentary layers. Presence of fine sediments within the events layers have been found in washovers deposited over low-energy, organic-rich back-barrier areas, where post-depositional bioturbation tends to mix sand and fine-grained deposits (Sedgwick and Davis, 2003). Finally, the presence of fine-grained material may also be linked to resuspension of back-barrier fine sediments caused by storm driven agitation (Kongsen *et al.*, 2021), to post-

depositional processes (percolation of fines throughout sandy layers) or to the reworking of marsh back-barrier sediments by flow conditions (Sedgwick and Davis, 2003).

In a northern lagoonal saltmarsh such as Penouille, the presence of sand within marsh sediments could also be related to ice-rafting, which has been suggested to be an important winter sedimentation process bringing sand material up to the high-marsh areas during spring tides and winter storms ( Dionne, 1989; Argow *et al.*, 2011; FitzGerald *et al.*, 2020). The fact that coarse layers found in Penouille marsh cores can be traced across the marsh cannot really be used as an argument to discard ice-rafting since, even if most ice-rafted deposits are reported to be clumpy and of meter-scale (e.g. Dionne, 1989), evidences were reported of ice-rafted mats continuously covering very extensive areas (e.g. Fitzgerald *et al.*, 2020) yet in much larger and more open lagoonal areas than Penouille. The grain-size signature of cores sand layers is a more conclusive argument. Ice-rafts anchors at low-tide on tidal flats and within the marsh creeks before being lifted up when the tide comes in. Ice-rafted deposits thus share a sedimentological signature with their source areas, while furthermore often presenting complex facies of mixed mud, sand, gravel, organics and shell components (e.g. Argow *et al.*, 2011). Results obtained by Gibeault *et al.* (2016) showed the sand component of Penouille tidal flat and lagoon sediments to be unimodal with a gaussian-like distribution centered around 1.5 phi (Gibeault, 2013). Such grain-size signature is very alike the one we obtained for the basal sand layer of core PEN-ST3-1 (gaussian-like distribution centered around 340 to 370 µm, 1.3 to 1.5 phi, Fig. 6) but otherwise share little similarities with the pluri-modal grain-size distribution (bi-modal within the range of sand material) of the event layers found above within the marsh succession (Fig. 6), thus somehow discarding the ice-rafting hypothesis. Finally, a last hypothesis could be that part of the sand material present in Penouille internal marshes could originate from the erosion of the sandy micro-cliffs located west of the marsh areas (Fig. 12-C-D-E) during periods of elevated water level in the lagoon, as showed by the presence of eastward-directed small secondary spits signs of a longshore transit of sand material towards the inner-parts of the lagoon (Gibeault, 2013). Easterly storms of December 2016 were witnessed to have caused the

deposition of sand within the internal marsh areas by storm waves having refracted around the peninsula. Deciphering between these and overwash inputs is rather difficult since both carry similar sand material originating from the beach and nearshore domains (the micro-cliffs being cut in the former beach-ridges composing the Penouille spit). Yet, the fact that the material of coarse sedimentary beds is well-sorted and carries a fair amount of fine sand gives credits to the latter hypothesis.

**6.1.2. Sandy Beach marsh**

At Sandy Beach, storm-driven submersions are the main, if not the only provider of coarse sedimentation to the marsh areas behind. All storms listed in the archive caused storm water-level to overtop the barrier crest and deposit extensive overwash deposits over the back-barrier marshes (or even cause the complete inundation of the system, e.g. storm of December, 1983), such as shown by oblique pictures taken at Sandy Beach before and after the storm of 30 December 2016 (Fig. 12-II). The characteristics of the coarse sediment beds shows an excess of coarse particle in the event beds and advocate for deposition under high-energy processes such as storm-induced overwashes (Fig. 10). The dispersion in sorting values also points towards that direction (Fig. 10). Washover deposits have been repeatedly observed to carry fuzzy sorting signatures (Kongsen et al., 2021; Switzer and Jones, 2008) either caused by the mixing of sediments from the nearshore, shoreface, beach and dune environments within the washover fluxes or to post-depositional processes reworking the washover deposit after hand (such as the selective removing of material or winnowing by aeolian processes or subsequent overwash fluxes, e.g. Sedgwick and Davis, 2003). The washover origin of the events beds found in core SB-STM-1 is further confirmed by the close proximity of these latter with sediments sampled at the surface of a washover lobe deposited close to the coring site by a 2016 storm (Fig. 10). Most event beds identified within core SB-STM-1 can be followed laterally and traced down with reasonable reliability within cores SB-STM-2 and SB-STM3 (Fig. 8) The shift observed in the position of Zr on the PCA's dimension from an association with coarse-grained associated variables in the seaward cores to an association with fine-grained linked variables in the most

landward core can be seen as the progressive settling of heavy mineral particles as overwash fluxes vanished over the marsh. All This reinforce the assertion that coarse sedimentary layers in core SB-ST-M1 originate from overwash dynamics caused by easterly storm events.

**6.2. Records of coarse sedimentary events and inter-site variability**

The temporal resolution of the two sedimentary archives differs, as well as does the respective sensitivity of each site to submersion processes, in turn influencing the frequency of coarse sedimentary events reconstructed at each site. The mean sedimentation rate at Penouille over the length of the reconstruction was 1.5 ± 0.38 mm.yr-1, compared to 0.69 ± 0.44 mm.yr-1 at Sandy Beach, thus allowing the record of sedimentary events at Penouille to be better separated and preserved. The higher temporal resolution at Penouille allowed for the identification of 17 events between 1600 C.E. and present day, compared to only 9 events reconstructed at Sandy Beach (Fig. 3; fig. 7; Table 4). Despite this difference in resolution and event frequency, there is a good general coherence between the two records (Fig. 14; Table 4). The coherence in event variability within the records also coincides with historical events recorded within the literature (Bernatchez *et al.*, 2012; Table 4). For example, the submersion event recorded at Penouille in 1877 C.E. (± 19 years), and at Sandy Beach at 1891 C.E. (± 19 years), most likely coincides with the event of 5 November 1884 which caused widespread damage at the regional scale associated with several shipwrecks (Bernatchez *et al.*, 2012). Similar coherence of the sedimentary record with events listed in the historical chronicles is true for the 20$^{th}$ century (Table 4), though with lesser accuracy. Some historical storm events are not present within the sedimentary record, and likewise, some reconstructed events are not ubiquitous within historical archives such as the ones observed during the 1940s in both PEN-ST3-1 and SB-STM-1 cores. Known (historical) storm events may be absent from the sedimentary record due to, for example, (i) to parameters inherent to storms themselves, such storm waves of direction non favorable to the penetration of the waves in the Gaspé Bay, storm wave conditions occurring at low tide, or because winter sea-ice cover may have been locally too massive and dampened storm-waves at the coast, or (ii) to the dynamic nature of barrier and back-barrier

couples (e.g. changes in the barrier height and/or in the accommodation space available in the marsh area) that conditions the occurrence of washovers at the coring site as well at its subsequent preservation in the sedimentary archives (Goslin and Clemmensen, 2017). In Sandy Beach for instance, the transgressive functioning of the sites implies that the shoreline has continuously retreated with time (over 1.5 m. yr-1 over the last 60 years; driven by RSLR, a negative sediment budget and roll-over overwash dynamics), hence increasing the probability that overwash fluxes reached the coring sites (e.g. Scileppi and Donnelly, 2007). This would explain the increase in the frequency of coarse deposits after 1900 C.E. Conversely, submersion events recorded in the sedimentary archives but absent from the historical chronicles may have occurred in localized wave conditions (perhaps during high tides) that lacked regional impact. Additionally, once a barrier has experienced an overwash event, the site can become more susceptible to overwash deposition outside of storm conditions due to persistent channels and lowered dune elevation (Donnelly *et al.*, 2001; Morton, 2002; Matias *et al.*, 2013; Rodrigues *et al.*, 2020), hence likely artificially increasing the numbers of deposits susceptible to be interpreted as storm washovers.

**6.3. Periodicity in the deposition of coarse sediments to the marshes**

Periodicities of ~130-140, ~90, ~50 and ~18-18.5 years were identified in $D_{90}$ grain-size time-series extracted from Penouille and Sandy Beach reference cores (Fig. 11). Periodic presence of coarse sediments within back-barrier marsh sedimentary succession have to be sought within cyclic behaviors of the water-level, for example due to climatically-driven changes in sea-level or storminess activity (Kolker *et al.*, 2009), linked to variations in Atlantic scale baroclinic gradients controlled by atmospheric and intra-oceanic dynamics (NAO, AMO and AMOC triplet). Centennial-scale periodicities found within our grain-size records may thus be the expression of these long-term climatically-driven sources of water-level variability. The 140-130-yr, 90-yr and 50-yr periodicities found within our records were repeatedly associated in the literature with multidecadal Atlantic climate variability (e.g. Mann et al., 2009; Ólafsdóttir et al., 2013; Wang et al., 2017).These were shown to be a prime control of sea-level variation on the North American eastern seaboard (Saher *et*

*al.*, 2015; Woodworth *et al.*, 2017; Kemp *et al.*, 2018) and more closely in Eastern Québec (Barnett *et al.*, 2019), but direct evidences of their effect on salt marsh sedimentation are only few and essentially reported from saltmarshes bounding the North Sea. Bartholdy *et al.* (2004) showed accretion rates in the Skalligen back-barrier marsh to be highly positively correlated to variations of the NAO winter index. Other studies identified NAO and AMOC-like cyclicities in North Sea saltmarsh sedimentary archives of past storminess (Bunzel *et al.*, 2021). Ocean-atmosphere modes of variability, and especially the NAO, were proposed modulate sediment supply to the marshes through the changes in storminess activity (French, 2006) and associated enhancement of the minerogenic inputs to the marshes these provoke (Kolker *et al.*, 2009; Baustian and Mendelssohn, 2015; Schuerch *et al.*, 2012, 2018a; Castagno *et al.*, 2018).

The ~18.5-yr periodicity found within the Penouille record and, to a lesser extent, the ~18-yr wavelength identified in Sandy Beach grain record both evoke the 18.61-yr low frequency periodicity of the nodal tidal cycle. The nodal tidal cycle is responsible for the periodic raising and lowering of mean high tide level (Woodworth, 1999; Gratiot *et al.*, 2006; Shaw and Tsimplis, 2010; Haigh *et al.*, 2011; Peng *et al.*, 2019) and has been shown to play a major role in the multi-decadal evolution of coastal morpho-sedimentary systems and in the return-periods of high-water (Oost *et al.*, 1993; Gratiot *et al.*, 2006; Baart *et al.*, 2012; Levoy *et al.*, 2017; Tessier *et al.*, 2019) throughout the effects it has on tidal sedimentation (French *et al.*, 2006). The exact mechanism by which the nodal tidal cycle has influenced coarse-sedimentation event occurrence at our study sites remains difficult to define. Modelling work of French (2006) showed how small variations in tidal amplitude controlled by the 18.6-yr nodal tidal cycle could drive considerable variations in hydroperiod in the upper intertidal marsh domains (frequency and duration of the tidal inundation), and in turn be responsible for sub-centimeter-scale variations in the sedimentation rates in these areas. At Penouille, the open-configuration of the back-barrier area makes it possible that periods of enhanced high-tide high-water levels may favor both extended hydroperiods upon the marsh areas as well as the reactivation or the sandy micro-cliffs on the inner side of the Penouille spit and contribute this way to supply the

marsh with coarse sediment without the need for storm conditions to happen. In Sandy Beach however, given the enclosed configuration of the marsh and the very internal, rarely flooded, position of the coring location, the ~18-yr periodicity identified in the record of coarse-grain sedimentation appear to be more likely only relatable to overwash dynamics and thus questions the role played by the nodal tidal cycle in the occurrence of washover deposits. The possibility of a linkage between the two processes has been recognized by Tessier *et al.* (2019) in the hypertidal Mont-Saint-Michel Bay (NW France), where the 18.6-yr tidal cycle was clearly observed to control the occurrence of washovers upon shelly beach ridges systems as well as the accumulation of coarse-grained sediments in the flat areas. Yet, translating these results into a microtidal context such as the bay of Gaspé appears rather questionable. Using the empiric linear relationship between tidal-range and the amplitude of the modulation caused by the 18.6-yr nodal cycle proposed by Peng *et al.* (2019) for a variety of tidal configurations, we calculated that in the Gaspé Bay (semi-diurnal location; 1.7 m tidal range), the 18.6-yr cycle could likely cause modulations of only 2 to 7 cm of the 99$^{th}$ percentile MMHW tidal amplitude. Whether the variations in tidal amplitude driven by the nodal tidal cycle would be sufficient to facilitate the occurrence of submersions during the peaks and thus accelerate the overtopping of the barriers by storm-surges is dubious, and would have to be further tested in a future study. Still, our results highlight that the nodal tidal cycle likely plays an important role in the high-frequency variability of coarse-sedimentation - and likely submersion event-occurrence in back-barrier marshes. But our data also show that this high frequency signal is superimposed on a lower, centennial to pluri-centennial, signal for which long term RSL changes and variability in sediment accretion rates are good candidates.

**6.4. Vertical marsh accretion: long-term RSL vs. sediment supply**

Along with vegetation dynamics and organic matter accretion, RSL changes and sediment supply are two of the main factors which, by governing the accommodation space available in the back-barrier area, participate in controlling the general vertical accretion of back-barrier salt-marshes and determines their ability to keep pace with RSLR (Allen, 2000). An ongoing scientific debate has been

to determine whether saltmarshes would die and shrunk from RSLR or on the contrary be able to keep up with it and even expand (Kirwan *et al.*, 2016), and under which physiographic and eco-geomorphic conditions one or the other outcome would prevail. Differences between minerogenic and organogenic marshes were repeatedly reported, the latter being more likely to withstand RSLR thanks to vegetation growth and associated positive sedimentation feedback loops, while the behavior of minerogenic marshes would heavily rely on sediment supply.

Figure 13-I shows the accretion histories of both Penouille and Sandy Beach against the mean rate of RSLR from the closest available record of Baie-des-Chaleurs (Barnett *et al.*, 2019). Penouille and Sandy Beach marshes broadly accreted simultaneously to RSLR (Fig.13-I). Yet, in detail, we see that the accretion histories of the two marshes varied considerably in rates and followed desynchronized timings (Fig. 13-I and III). Considering the proximity of the two marshes, this illustrates how mean RSLR alone cannot satisfyingly explain the accretion of back-barrier marshes. Numerous observational and modelling studies demonstrated that the behavior of sandy barrier/marsh couples to RSLR indeed depends on a complex assemblage of factors conditioning the overall sediment budget of the system and its capability to adapt to RSLR (Cooper *et al.*, 2018; Fruergaard *et al.*, 2020). Opposite chronologies of deposition rates were experienced by the surface of the two studied marshes (Fig. 13-III). Changes in elevation of the Penouille marsh followed three periods (1620-1730, 1730-1870 and 1870-2018) characterized by distinct rhythms of accretion of 1.45±0.1 mm. $yr^{-1}$, 1.68±0.28 mm. $yr^{-1}$ and 0.93±0.28 mm. $yr^{-1}$, respectively (Fig. 13-I and III). Until 1890, Penouille experienced accretion rates greater than contemporaneous RSL rise, supported by high deposition rates (Fig. 13-III). As a result, Penouille marsh followed a sustained aggradation allowing the marsh to largely withstand RSLR (Fig. 13-IV). Accretion rate dropped considerably at the beginning of the 20$^{th}$ century, hence so did the rhythm of aggradation of the marsh which then entered a near stable to submerging state (Fig. 13-IV). Interestingly, 1870 C.E. is the time at which a transition from a low- to mid-marsh to a high-marsh deposit environment occurred at the location of core PEN-ST3-1 (expressed by a sharp increase in organic content from ~20 % to 40-60 %, Fig. 3). In

other terms, it means that the surface of Penouille marsh accreted at rates greater than RSLR, whereas in the lower marsh domain before getting back to rates equivalent or lower to RSLR when high-marsh conditions got established. This is in line with the traditional paradigm that is that sedimentation and aggradation rates drop as marshes reach maturity, therefore making them *a priori* more vulnerable to any subsequent RSL rise (Allen, 2000), as well as with the results of some observational studies (Blum *et al.*, 2012) and meta-analyses obtained (Kirwan *et al.*, 2016) that showed accretion rates to be generally slightly higher in the low- than in the high-marsh domains. At Sandy Beach, the marsh at the location of core SB-STM-1 first elevated at a much slower rate (0.47±0.09 mm. $yr^{-1}$) than RSL rise (Fig. 13-I and III). It then elevated rapidly during the 1906-1984 C.E. period (1.46±0.28 mm. $yr^{-1}$), supported by a sharp increase in deposition rates (Fig. 13-III). This allowed Sandy Beach marsh to get out of its submerging state and to enter an aggrading behavior allowing it to keep up with RSLR (Fig. 13-IV). Nonetheless, in complete opposition to what was observed for Penouille marsh, the period of accelerated accretion at Sandy Beach marsh is synchronous with the onset of a very organic high-marsh sedimentation at the location of core SB-STM-1 (Fig. 7), hence apparently in contradiction with the classic paradigm introduced above of reduced sedimentation and accretion rates within high-marshes areas.

To better understand the drivers of sediment deposition at the surface of the two marshes, we decomposed total deposition rates in mineral and organic deposition rates. In Penouille, organogenic deposition explain significant amounts of the overall deposition rate in both periods of reduced and elevated minerogenic deposition, hence showing the marsh to be predominantly organogenic (Fig. 14-A). However, minerogenic deposition explain most of the overall deposition rate in period of elevated deposition, showing the marsh to also heavily depend on minerogenic in puts to accrete (Fig. 14-A). In Sandy beach on the contrary, we see minerogenic deposition to explain most of the overall deposition in both periods of reduced and elevated minerogenic deposition, hence classifying the marsh as predominantly minerogenic (Fig. 14-B). Yet, during periods of reduced minerogenic deposition at this marsh, we see a significant amount of the overall deposition to be also explained

by organogenic accretion, showing the return to an important role played by vegetation-controlled accretion of the marsh during periods of reduced minerogenic inputs (Fig. 14-B).

Fast accretion rates known by Penouille marsh over the 1620-1870 C.E. period were supported by high minerogenic sediment deposition rates (Fig. 13-III and V). It is also evident that the drop in accretion rates observed around 1870 C.E. (Fig. 13-III) find its roots in a sudden decrease in minerogenic deposition at the surface of the marsh (Fig. 13-V), since organic accretion have remained rather stable across the whole study period. Hence, in Penouille, organic deposition, such as supplied by autochthonous in-situ plant growth and litter degradation in the high-marsh domain was insufficient to counteract the drop in minerogenic sediment supply. In Sandy Beach, the large increase in accretion rates experienced from ~1900 C.E. seems to have been driven by both an increase in minerogenic inputs (mainly) and to a lesser extent in organogenic deposition (Fig. 13-VI). The striking similarity between the rise in accretion rates at the surface of Sandy Beach marsh and the sudden increase in minerogenic sedimentation (Fig. 13-III and VI) clearly demonstrates the role played by inorganic sedimentation in the aggrading capacity the otherwise submerging Sandy Beach marsh acquired during the 20$^{th}$ century (Fig. 13-IV). These results thus show that minerogenic deposition have clearly conditioned the accretion behaviors and capabilities of adaptation of both studied marsh to RSLR (Fig. 13-V and VI), as repeatedly observed worldwide in other minerogenic marshes (e.g. Kolker *et al.*, 2010; Fitzgerald and Hughes, 2019). This furthermore confirms how dependent low tidal range low sediment supply marshes are to minerogenic sedimentary inputs regarding their aptitude to withstand RSLSR (e.g. Kirwan *et al.*, 2010). As for Sandy Beach, knowing the large sedimentary deficit in which the barrier is (section 5.1, Fig. 2-B), the sudden rise in minerogenic input observed after 1900 C.E. also sheds light on the role event-driven sedimentation (such as storm events) may play in maintaining microtidal marshes capabilities to keep up with RSLR.

**6.5. Coarse minerogenic sedimentation in the resilience of salt-marshes to RSLR**

Penouille and Sandy beach marshes being mostly minerogenic marshes, established in microtidal conditions and in sedimentary deficit, we ought to test in which measure the coarse sediments (brought by storm events in Sandy Beach and likely to be for most of them in Penouille) observed within the sedimentary archives (see section 5.2.4 and 5.3.4, Fig. 3 and 7) would explain the variations in minerogenic sedimentation and associated accretion rates observed for the two marshes. We tested separately the relationships between coarse sedimentation and minerogenic deposition for the periods during which minerogenic inputs to both marshes were considerable and caused aggradation of both marsh surfaces (Pre-1870 C.E. period for Penouille, Post-1900 C.E. period for Sandy Beach) and for periods during which reduced minerogenic deposition caused the marshes to be submerged (Fig. 13, Fig. 15). In Penouille (aggradational barrier), coarse sedimentary layers do not seem to have caused clear and significant departures of the deposition rates from the rates associated with the modal marsh fine-grained sedimentation during periods of either high or low minerogenic deposition upon the marsh (after 1870 C.E., Fig. 13-V; Fig. 15-A). For periods of high minerogenic deposition, no significant relationship is observed between minerogenic deposition rates and the percentages of abnormally coarse sedimentary material (Fig. 15-B, coarse referring to the grain-size fractions showing the highest downcore grain-size standard deviation; see section 4.2.4, here the fraction > 213 µm for Penouille, Fig. 3-D). On the contrary, during periods of reduced minerogenic deposition (post 1870 C.E.), inputs of coarse sediments take importance and explain a significant and considerable part of the minerogenic deposition upon the marsh ($R^2$= 0.30; $p$= 0.048, Fig. 15-B). This would mean that before 1870 C.E., while minerogenic deposition rates were high at this site, fine-grained and coarse minerogenic deposition were in equilibrium and concurred to raise the marsh surface. This occurred while the coring site was a low-to mid-marsh environment, hence concerned with tidally-derived deposition. The drop of minerogenic deposition from 1870 and onwards is linked to the onset and expansion of the high-marsh domain at the expense of the low marsh, in line with recent surface analysis. Organogenic-driven accretion of the marsh became much slower at this point, so that event-based coarse minerogenic beds gained importance point in

explaining minerogenic accretion rates of the marsh. Despite the acceleration of RSLR observed in the region since the end of the 1980s (Gibeault *et al.*, 2016), we find that the accretion of Penouille marsh has been sufficient to allow its surface area to remain stable. Hence, these results show that in Penouille event-driven coarse minerogenic sedimentation became salutary in maintaining the capacity of the marsh to stay in equilibrium with RSLR whereas the marsh shifted from minerogenic to organogenic deposition. Coarse sediment deposition at this site having closely followed the ~18.6-year tidal cycle (see sections 5.4 and 6.3), the frequency of coarse sedimentation upon the marsh has likely been sufficiently spaced in time to allow marsh vegetation to develop upon them, promoting the durability of the barrier/marsh couple equilibrium through a symbiotic feedback (Walters *et al.*, 2014).

Contrary is observed for Sandy Beach (transgressive barrier). Here, coarser minerogenic sedimentation is observed to globally cause deposition rates higher than the rates of accumulation permitted by modal marsh sedimentation during periods of elevated marsh accretion rates (Fig. 15-C). This goes along with a fair amount (27 %) of minerogenic deposition rates being explained by percentages of coarse sedimentary fraction ($R^2$= 0.27, $p$= 0.04, Fig. 15-D). This well corresponds to the incorporation of important amounts of allochthonous sand material upon the modal marsh domain by washover deposits. As for Sandy Beach, submersion episodes are the main process allowing the internal and upper domains of the marsh normally concerned with very limited accretion of fine tidally-derived sedimentary inputs to develop vertically. At this site, the results we obtained confirm that washover deposits and storm-related minerogenic deposition play a central role in allowing the most internal/mature sectors of the marshes to aggrade and as a consequence in giving transgressive barrier/marsh couples the capacity to be resilient to RSLR. This goes well with the idea that arised rather recently in the literature that high-energy events may be beneficial rather than detrimental for the capacity of saltmarshes to face RSLR thanks the substantial net sediment inputs brought by storm surges, either frontally by means of overwash deposition (Schuerch *et al.*, 2012) or throughout an enhanced circulation of water fluxes loaded with suspended material in tidal

inlets and back-barrier lagoons (Castagno *et al.*, 2018). Such storm-driven minerogenic sedimentary inputs are especially redeeming for systems facing sedimentary deficit (Cahoon *et al.*, 2006) and even more in microtidal systems for which short-term storm-driven elevations of the water level raise the tidal range by several order of magnitude and thus authorize sediments to be deposited in rarely flooded high-marsh areas, hence considerably promoting the accretion of the marshes (Allen, 2000; Kolker *et al.*, 2009) and boosting the capability of marshes to keep up with RSLR (Kirwan *et al.*, 2010 and this study, see above section 6.4).

All-in-all, the results obtained in the present study suggest that to improve the resilience of microtidal coastal marshes to ongoing RSL rise, would the latter be minerogenic or organogenic, transgressive or aggradationnal, it appears essential that the natural ability of coarse sedimentation to enter back-barrier saltmarshes, either by means of overwash dynamics and /or through remobilization of lagoonal material is maintained. Where occulted by anthropogenic intervention, it is advised that the connections between the beach-dune and marsh domains are restored.

## 5.CONCLUSION

We reconstructed the chronology of coarse sedimentation over the past centuries at two back-barrier saltmarshes of the Bay of Gaspé (Eastern Canada), established behind transgressive and aggradationnal sand barriers, respectively. The joint use of sedimentological and geochemical markers allowed us to build records of coarse sedimentary deposition that affected the two marshes between 1620-2018 C.E. In Sandy Beach marsh (transgressive system), coarse sedimentary events can only originate from washover deposition during intense storm events. In Penouille (aggradationnal system), a dual origin is proposed for the coarse sedimentation: overwash dynamics and remobilization of internal lagoon sand material (or most likely from the combination of the two processes during storm events). Time-series analyses of the $D_{90}$ coarse sedimentation record show the existence of pluri-decadal cyclicities typical of controls exerted by climatic atmospheric and intra-oceanic modes of variability on water-level, as well as a 18 to 18.5-yr cyclicity strongly evoking the

18.61-yr nodal tidal cycle, especially prominent in Penouille still identifiable and significant in Sandy beach. This suggests that the lunar periodic modulation of the tidal amplitude may have been paramount in fostering the occurrence of coarse sedimentary events upon the marshes. In Penouille marsh, where the marsh fringes a sandy back-barrier lagoon, it is possible that the nodal tidal cycle may favor coarse sedimentation in the upper parts of the marsh by considerably boosting the hydroperiod in these domains and allowing the reworking of the back-barrier microcliffs which are entailed into former beach-ridges. This does not stand true for the Sandy beach marsh, which is located in the very internal part of a marsh enclosed between a double spit system and far from tidal channels. For the latter, we assume that the variations in tidal amplitude driven by the nodal tidal cycle may play a role in promoting the deposition of coarse material upon the marsh throughout a facilitation of storm- or non-storm driven washover events. Based on available models, we estimate that the modulation of the tidal amplitude provoked by the nodal tidal cycle to likely represent only a 2 to 7 cm increase of the water-level elevation. This calls for the nodal tidal cycle to be better implemented in the design of adaptation strategies for coastal areas.

Secondly, we put the records of marsh coarse sedimentation in perspective with the accretion histories of the two marshes and their behavior in a regime of relative sea-level rise. Results show that punctual coarsesediment deposition has been, and still is, crucial in maintaining the capacity of the two marshes to withstand RSLR. As for the transgressive site, we find that coarse event-driven minerogenic deposition actively participated in fueling minerogenic deposition in the marsh over the last century, hence raising the otherwise submerging marsh surface and providing it the capacity to keep up with RSLSR. At the aggradationnal site, we show that coarse sedimentation upon the back-barrier marshes did not boost accretion rates during periods which minerogenic deposition rates upon the marsh were already high. But coarse sedimentation became crucial as soon as high-marsh conditions got established and the site shifted from a minerogenic to an organogenic functioning. Coarse sediments then began to represent a significant part of the minerogenic deposition to the marsh, allowing the latter to keep pace with RSLR. All-in-all, our results demonstrate that coarse

event-driven minerogenic deposition upon microtidal minerogenic or organogenic back-barrier saltmarshes is crucial for maintaining the capacity of the marshes to cope with relative sea-level rise. Where occulted by anthropogenic intervention, it is advised that the natural ability of coarse sedimentation to enter back-barrier saltmarshes is restored and connections between the beach-dune and marsh domain kept maximal. This information is essential to identify near-term restoration and conservation measures that will be adequate.

**Acknowledgement**

This work was funded by the Coastal Geoscience Chair at the Université du Québec at Rimouski as part of the Québec Government initiative on natural risks prevention and the Plan d'action 2013–2020 sur les changements climatiques et du Fonds Vert. All data will be made available through the SEANOE repository following publication, with the following DOI: https://doi.org/10.17882/80577

**References**

Allard Michel ; Tremblay, G., 1981. Observations sur le Quaternaire de l'extrémité orientale de la péninsule de Gaspé, Québec. Géographie Phys. Quat. 35, 105–125. https://doi.org/https://doi.org/10.7202/1000382ar

Allen, J.R.L., 2000. Morphodynamics of Holocene salt marshes: A review sketch from the Atlantic and Southern North Sea coasts of Europe. Quat. Sci. Rev. 19, 1155–1231. https://doi.org/10.1016/S0277-3791(99)00034-7

Appleby, P.G., Oldfield, F., 1978. The calculation of lead-210 dates assuming a constant rate of supply of unsupported 210Pb to the sediment. CATENA 5, 1–8. https://doi.org/https://doi.org/10.1016/S0341-8162(78)80002-2

Argow, B.A., Hughes, Z.J., FitzGerald, D.M., 2011. Ice raft formation, sediment load, and theoretical potential for ice-rafted sediment influx on northern coastal wetlands. Cont. Shelf Res. 31, 1294–1305. https://doi.org/10.1016/j.csr.2011.05.004

Arias-Ortiz, A., Masqué, P., Garcia-Orellana, J., Serrano, O., Mazarrasa, I., Marbà, N., Lovelock, C.E., Lavery, P.S., Duarte, C.M., 2018. Reviews and syntheses: \chem{^{210}Pb}-derived sediment and carbon accumulation rates in vegetated coastal ecosystems -- setting the record straight. Biogeosciences 15, 6791–6818. https://doi.org/10.5194/bg-15-6791-2018

Baart, F., Van Gelder, P.H.A.J.M., De Ronde, J., Van Koningsveld, M., Wouters, B., 2012. The effect of the 18.6-year lunar nodal cycle on regional sea-level rise estimates. J. Coast. Res. 28, 511–516. https://doi.org/10.2112/JCOASTRES-D-11-00169.1

Barbier, E.B., Hacker, S.D., Kennedy, C., Koch, E.W., Stier, A.C., Silliman, B.R., 2011. The value of estuarine and coastal ecosystem services. Ecol. Monogr. 81, 169–193. https://doi.org/https://doi.org/10.1890/10-1510.1

Barnett, R.L., Bernatchez, P., Garneau, M., Brain, M.J., Charman, D.J., Stephenson, D.B., Haley, S., Sanderson, N., 2019. bec and potential Late Holocene sea-level changes in eastern Qu e drivers. Quat. Sci. Rev. 203, 151–169. https://doi.org/10.1016/j.quascirev.2018.10.039

Bartholdy, J., Christiansen, C., Kunzendorf, H., 2004a. Long term variations in backbarrier salt marsh deposition on the Skallingen peninsula - The Danish Wadden Sea. Mar. Geol. 203, 1–21. https://doi.org/10.1016/S0025-3227(03)00337-2

Bartholdy, J., Christiansen, C., Kunzendorf, H., 2004b. Long term variations in backbarrier salt marsh deposition on the Skallingen peninsula - The Danish Wadden Sea. Mar. Geol. 203, 1–21. https://doi.org/10.1016/S0025-3227(03)00337-2

Baskaran, M., Naidu, A.S., 1995. 210Pb-derived chronology and the fluxes of 210Pb and 137Cs isotopes into continental shelf sediments, East Chukchi Sea, Alaskan Arctic. Geochim. Cosmochim. Acta 59, 4435–4448. https://doi.org/https://doi.org/10.1016/0016-7037(95)00248-X

Baustian, J.J., Mendelssohn, I.A., 2015. Hurricane-Induced Sedimentation Improves Marsh Resilience and Vegetation Vigor under High Rates of Relative Sea Level Rise. Wetlands 35, 795–802. https://doi.org/10.1007/s13157-015-0670-2

Bernatchez, P., 2013. Dynamique de l'écosystème côtier de la péninsule de Penouille dans un contexte de changements climatiques, Parc national du Canada Forillon.

Blott, S.J., Pye, K., 2001. GRADISTAT: a grain size distribution and statistics package for the analysis of unconsolidated sediments. Earth Surf. Process. Landforms 26, 1237–1248. https://doi.org/https://doi.org/10.1002/esp.261

Bunzel, D., Milker, Y., Müller-Navarra, K., Arz, H.W., Schmiedl, G., 2021. North Sea salt-marsh archives trace past storminess and climate variability. Glob. Planet. Change 198, 103403. https://doi.org/10.1016/j.gloplacha.2020.103403

Cahoon, D.R., Hensel, P.F., Spencer, T., Reed, D.J., McKee, K.L., Saintilan, N., 2006. Coastal Wetland Vulnerability to Relative Sea-Level Rise: Wetland Elevation Trends and Process Controls, in: Verhoeven, J.T.A., Beltman, B., Bobbink, R., Whigham, D.F. (Eds.), Wetlands and Natural Resource Management. Springer Berlin Heidelberg, Berlin, Heidelberg, pp. 271–292. https://doi.org/10.1007/978-3-540-33187-2_12

Castagno, K.A., Jiménez-Robles, A.M., Donnelly, J.P., Wiberg, P.L., Fenster, M.S., Fagherazzi, S., 2018. Intense Storms Increase the Stability of Tidal Bays. Geophys. Res. Lett. 45, 5491–5500. https://doi.org/10.1029/2018GL078208

Cattrijsse, A., Hampel, H., 2006. European intertidal marshes: A review of their habitat functioning and value for aquatic organisms. Mar. Ecol. Prog. Ser. 324, 293–307. https://doi.org/10.3354/meps324293

Cazenave, A., Cozannet, G. Le, 2014. Sea level rise and its coastal impacts. Earth's Futur. 2, 15–34. https://doi.org/https://doi.org/10.1002/2013EF000188

Clemmensen, L.B., Glad, A.C., Kroon, A., 2016. Storm flood impacts along the shores of micro-tidal inland seas: A morphological and sedimentological study of the Vesterlyng beach, the Belt Sea, Denmark. Geomorphology 253, 251–261. https://doi.org/10.1016/j.geomorph.2015.10.020

Cooper, J.A.G., Green, A.N., Loureiro, C., 2018. Geological constraints on mesoscale coastal barrier behaviour. Glob. Planet. Change 168, 15–34. https://doi.org/https://doi.org/10.1016/j.gloplacha.2018.06.006

Crosby, S.C., Sax, D.F., Palmer, M.E., Booth, H.S., Deegan, L.A., Bertness, M.D., Leslie, H.M., 2016. Salt marsh persistence is threatened by predicted sea-level rise. Estuar. Coast. Shelf Sci. 181, 93–99. https://doi.org/https://doi.org/10.1016/j.ecss.2016.08.018

Didier, D., Bandet, M., Bernatchez, P., Dumont, D., 2019. Modelling Coastal Flood Propagation under Sea Level Rise: A Case Study in Matia, Eastern Canada. Geosciences 9. https://doi.org/10.3390/geosciences9020076

Dionne, J.-C., n.d. An Estimate of Shore Ice Action in a Spartina Tidal Marsh, St. Lawrence Estuary, Québec, Canada on JSTOR.

Donnelly, J.P., Roll, S., Wengren, M., Butler, J., Lederer, R., Webb, T., 2001. Sedimentary evidence of intense hurricane strikes from New Jersey. Geology 29, 615–618. https://doi.org/10.1130/0091-7613(2001)029<0615:SEOIHS>2.0.CO;2

FitzGerald, D.M., Fenster, M.S., Argow, B.A., Buynevich, I. V, 2008. Coastal Impacts Due to Sea-Level Rise. Annu. Rev. Earth Planet. Sci. 36, 601–647. https://doi.org/10.1146/annurev.earth.35.031306.140139

Fitzgerald, D.M., Hughes, Z., 2019. Marsh processes and their response to climate change and sea-level rise. Annu. Rev. Earth Planet. Sci. 47, 481–517. https://doi.org/10.1146/annurev-earth-082517-010255

FitzGerald, D.M., Hughes, Z.J., Georgiou, I.Y., Black, S., Novak, A., 2020. Enhanced, Climate-Driven Sedimentation on Salt Marshes. Geophys. Res. Lett. 47, e2019GL086737. https://doi.org/10.1029/2019GL086737

Fox, W.T., Haney, R.L., Curran, H.A., 1995. Penouille Spit, evolution of a complex spit, Gaspe, Quebec, Canada. J. Coast. Res. 11, 478–493.

French, J., 2006. Tidal marsh sedimentation and resilience to environmental change: Exploratory modelling of tidal, sea-level and sediment supply forcing in predominantly allochthonous systems. Mar. Geol. 235, 119–136. https://doi.org/https://doi.org/10.1016/j.margeo.2006.10.009

Fruergaard, M., Sander, L., Goslin, J., Andersen, T.J., 2020. Temporary late Holocene barrier-chain deterioration due to insufficient sediment availability, Wadden Sea, Denmark. Geology 49, 162–167. https://doi.org/10.1130/G47978.1

Ganju, N.K., Defne, Z., Kirwan, M.L., Fagherazzi, S., D'Alpaos, A., Carniello, L., 2017. Spatially integrative metrics reveal hidden vulnerability of microtidal salt marshes. Nat. Commun. 8, 14156. https://doi.org/10.1038/ncomms14156

Ghaleb, B., 2009. Overview of the methods for the measurement and interpretation of short-lived radioisotopes and their limits. {IOP} Conf. Ser. Earth Environ. Sci. 5, 12007. https://doi.org/10.1088/1755-1307/5/1/012007

Gibeault, C., Neumeier, U., Bernatchez, P., 2016. Spatial and Temporal Sediment Dynamics in a Subarctic Salt Marsh (Gulf of St. Lawrence, Canada). J. Coast. Res. 32, 1344–1361. https://doi.org/10.2112/JCOASTRES-D-15-00160.1

Goslin, J., Clemmensen, L.B., 2017. Proxy records of Holocene storm events in coastal barrier systems: Storm-wave induced markers. Quat. Sci. Rev. 174, 80–119. https://doi.org/10.1016/j.quascirev.2017.08.026

Gratiot, N., Anthony, E.J., Gardel, A., Gaucherel, C., Proisy, C., Wells, J.T., 2006. Significant contribution of the 18 . 6 year tidal cycle to regional coastal changes 169–172. https://doi.org/10.1038/ngeo127

Gunnell, J.R., Rodriguez, A.B., McKee, B.A., 2013. How a marsh is built from the bottom up. Geology 41, 859–862. https://doi.org/10.1130/G34582.1

Haigh, I.D., Eliot, M., Pattiaratchi, C., 2011. Global influences of the 18.61 year nodal cycle and 8.85 year cycle of lunar perigee on high tidal levels. J. Geophys. Res. Ocean. 116. https://doi.org/10.1029/2010JC006645

Hinkel, J., Lincke, D., Vafeidis, A.T., Perrette, M., Nicholls, R.J., Tol, R.S.J., Marzeion, B., Fettweis, X., Ionescu, C., Levermann, A., 2014. Coastal flood damage and adaptation costs under 21st century sea-level rise. Proc. Natl. Acad. Sci. 111, 3292–3297. https://doi.org/10.1073/pnas.1222469111

Kemp, A.C., Wright, A.J., Edwards, R.J., Barnett, R.L., Brain, M.J., Kopp, R.E., Cahill, N., Horton, B.P., Charman, D.J., Hawkes, A.D., Hill, T.D., van de Plassche, O., 2018. Relative sea-level change in Newfoundland, Canada during the past ~3000 years. Quat. Sci. Rev. 201, 89–110. https://doi.org/10.1016/j.quascirev.2018.10.012

Kirwan, M.L., Temmerman, S., Skeehan, E.E., Guntenspergen, G.R., Fagherazzi, S., 2016. Overestimation of marsh vulnerability to sea level rise. Nat. Clim. Chang. 6, 253–260. https://doi.org/10.1038/nclimate2909

Kolker, A.S., Kirwan, M.L., Goodbred, S.L., Cochran, J.K., 2010. Global climate changes recorded in coastal wetland sediments: Empirical observations linked to theoretical predictions. Geophys. Res. Lett. 37, n/a-n/a. https://doi.org/10.1029/2010GL043874

Kongsen, S., Phantuwongraj, S., Choowong, M., 2021. Distinguishing Late Holocene Storm Deposit From Shore-normal Beach Sediments From the Gulf of Thailand. Front. Earth Sci. 9, 24. https://doi.org/10.3389/feart.2021.625926

Koohzare, A., Vaníček, P., Santos, M., 2008. Pattern of recent vertical crustal movements in Canada. J. Geodyn. 45, 133–145.

https://doi.org/https://doi.org/10.1016/j.jog.2007.08.001

Leonardi, N., Carnacina, I., Donatelli, C., Ganju, N.K., Plater, A.J., Schuerch, M., Temmerman, S., 2018. Dynamic interactions between coastal storms and salt marshes: A review. Geomorphology 301, 92–107. https://doi.org/10.1016/j.geomorph.2017.11.001

Levoy, F., Anthony, E.J., Dronkers, J., Monfort, O., Izabel, G., Larsonneur, C., 2017. Influence of the 18.6-year lunar nodal tidal cycle on tidal flats: Mont-Saint-Michel Bay, France. Mar. Geol. 387, 108–113. https://doi.org/10.1016/j.margeo.2017.03.009

Mann, M.E., Lees, J.M., 1996. Robust estimation of background noise and signal detection in climatic time series. Clim. Change 33, 409–445. https://doi.org/10.1007/BF00142586

Mann, M.E., Zhang, Z., Rutherford, S., Bradley, R.S., Hughes, M.K., Shindell, D., Ammann, C., Faluvegi, G., Ni, F., 2009. Global signatures and dynamical origins of the little ice age and medieval climate anomaly. Science (80-. ). 326, 1256–1260. https://doi.org/10.1126/science.1177303

Matias, A., Masselink, G., Kroon, A., Blenkinsopp, C.E., Turner, I.L., 2013. Overwash experiment on a sandy barrier. J. Coast. Res. 65, 772–783. https://doi.org/10.2112/si65-132.1

Mcleod, E., Chmura, G.L., Bouillon, S., Salm, R., Björk, M., Duarte, C.M., Lovelock, C.E., Schlesinger, W.H., Silliman, B.R., 2011. A blueprint for blue carbon: Toward an improved understanding of the role of vegetated coastal habitats in sequestering CO2. Front. Ecol. Environ. 9, 552–560. https://doi.org/10.1890/110004

Morton, R.A., 2002. Factors controlling storm impacts on coastal barriers and beaches - A preliminary basis for near real-time forecasting. J. Coast. Res. 18, 486–501.

Morton, R.A., Sallenger, A.H., 2003. Morphological impacts of extreme storms on sandy beaches and barriers. J. Coast. Res. 19, 560–573.

Ólafsdóttir, K.B., Geirsdóttir, Á., Miller, G.H., Larsen, D.J., 2013. Evolution of NAO and AMO strength and cyclicity derived from a 3-ka varve-thickness record from Iceland. Quat. Sci. Rev. 69, 142–154. https://doi.org/10.1016/J.QUASCIREV.2013.03.009

Oost, A.P., de Haas, H., Ijnsen, F., van den Boogert, J.M., de Boer, P.L., 1993. The 18.6 yr nodal cycle and its impact on tidal sedimentation. Sediment. Geol. 87, 1–11. https://doi.org/10.1016/0037-0738(93)90032-Z

Pendleton, L., Donato, D.C., Murray, B.C., Crooks, S., Jenkins, W.A., Sifleet, S., Craft, C., Fourqurean, J.W., Kauffman, J.B., Marbà, N., Megonigal, P., Pidgeon, E., Herr, D., Gordon, D., Baldera, A., 2012. Estimating Global "Blue Carbon" Emissions from Conversion and Degradation of Vegetated Coastal Ecosystems. PLoS One 7. https://doi.org/10.1371/journal.pone.0043542

Peng, D., Hill, E.M., Meltzner, A.J., Switzer, A.D., 2019. Tide Gauge Records Show That the 18.61-Year Nodal Tidal Cycle Can Change High Water Levels by up to 30 cm. J. Geophys. Res. Ocean. 124, 736–749. https://doi.org/10.1029/2018JC014695

Phantuwongraj, S., Choowong, M., Nanayama, F., Hisada, K.I., Charusiri, P., Chutakositkanon, V., Pailoplee, S., Chabangbon, A., 2013. Coastal geomorphic conditions and styles of storm surge washover deposits from Southern Thailand. Geomorphology 192, 43–58. https://doi.org/10.1016/j.geomorph.2013.03.016

Reimer, P.J., Bard, E., Bayliss, A., Beck, J.W., Blackwell, P.G., Ramsey, C.B., Buck, C.E., Cheng, H., Edwards, R.L., Friedrich, M., Grootes, P.M., Guilderson, T.P., Haflidason, H., Hajdas, I., Hatté, C., Heaton, T.J., Hoffmann, D.L., Hogg, A.G., Hughen, K.A., Kaiser, K.F., Kromer, B., Manning, S.W., Niu, M., Reimer, R.W., Richards, D.A., Scott, E.M., Southon, J.R., Staff, R.A., Turney, C.S.M., van der Plicht, J., 2013. IntCal13 and Marine13 Radiocarbon Age Calibration Curves 0–50,000 Years cal BP. Radiocarbon 55, 1869–1887. https://doi.org/10.2458/azu_js_rc.55.16947

Rodriguez, A.B., Theuerkauf, E.J., Ridge, J.T., VanDusen, B.M., Hagley, S.R., 2020. Long-term washover fan accretion on a transgressive barrier island challenges the assumption that paleotempestites represent individual tropical cyclones. Sci. Rep. 10, 1–10. https://doi.org/10.1038/s41598-020-76521-4

Sabatier, P., Dezileau, L., Colin, C., Briqueu, L., Bouchette, F., Martinez, P., Siani, G., Raynal, O., Von Grafenstein, U., 2012. 7000 years of paleostorm activity in the NW Mediterranean Sea in response to Holocene climate events. Quat. Res. 77, 1–11. https://doi.org/10.1016/j.yqres.2011.09.002

Saher, M.H., Gehrels, W.R., Barlow, N.L.M., Long, A.J., Haigh, I.D., Blaauw, M., 2015. Sea-level changes in Iceland and the influence of the North Atlantic Oscillation during the last half millennium. Quat. Sci. Rev. 108, 23–36. https://doi.org/10.1016/j.quascirev.2014.11.005

Schuerch, M., Dolch, T., Bisgwa, J., Vafeidis, A.T., 2018a. Changing sediment dynamics of a mature backbarrier salt marsh in response to sea-level rise and storm events. Front. Mar. Sci. 5, 1–14. https://doi.org/10.3389/fmars.2018.00155

Schuerch, M., Rapaglia, J., Liebetrau, V., 2012a. Salt Marsh Accretion and Storm Tide Variation : an Example from a Barrier Island in the North Sea 486–500. https://doi.org/10.1007/s12237-011-9461-z

Schuerch, M., Rapaglia, J., Liebetrau, V., Vafeidis, A., Reise, K., 2012b. Salt Marsh Accretion and Storm Tide Variation: An Example from a Barrier Island in the North Sea. Estuaries and Coasts 35, 486–500. https://doi.org/10.1007/s12237-011-9461-z

Schuerch, M., Spencer, T., Temmerman, S., Kirwan, M.L., Wolff, C., Lincke, D., McOwen, C.J., Pickering, M.D., Reef, R., Vafeidis, A.T., Hinkel, J., Nicholls, R.J., Brown, S., 2018b. Future response of global coastal wetlands to sea-level rise. Nature 561, 231–234. https://doi.org/10.1038/s41586-018-0476-5

Scileppi, E., Donnelly, J.P., 2007. Sedimentary evidence of hurricane strikes in western long Island, New York. Geochemistry, Geophys. Geosystems 8, 1–25. https://doi.org/10.1029/2006GC001463

Sedgwick, P.E., Davis, R.A., 2003. Stratigraphy of washover deposits in Florida: Implications

for recognition in the stratigraphic record. Mar. Geol. 200, 31–48. https://doi.org/10.1016/S0025-3227(03)00163-4

Shaw, A.G.P., Tsimplis, M.N., 2010. The 18.6 yr nodal modulation in the tides of Southern European coasts. Cont. Shelf Res. 30, 138–151. https://doi.org/10.1016/j.csr.2009.10.006

Shaw, J., Piper, D.J.W., Fader, G.B.J., King, E.L., Todd, B.J., Bell, T., Batterson, M.J., Liverman, D.G.E., 2006. A conceptual model of the deglaciation of Atlantic Canada 25, 2059–2081. https://doi.org/10.1016/j.quascirev.2006.03.002

St-Onge, G., Mulder, T., Francus, P., Long, B., 2007. Chapter Two Continuous Physical Properties of Cored Marine Sediments, in: Hillaire–Marcel, C., De Vernal, A. (Eds.), Proxies in Late Cenozoic Paleoceanography, Developments in Marine Geology. Elsevier, pp. 63–98. https://doi.org/https://doi.org/10.1016/S1572-5480(07)01007-X

Switzer, A.D., Jones, B.G., 2008. Large-scale washover sedimentation in a freshwater lagoon from the southeast Australian coast: Sea-level change, tsunami or exceptionally large storm? Holocene 18, 787–803. https://doi.org/10.1177/0959683608089214

Temmerman, S., Moonen, P., Schoelynck, J., Govers, G., Bouma, T.J., 2012. Impact of vegetation die-off on spatial flow patterns over a tidal marsh. Geophys. Res. Lett. 39, 1–5. https://doi.org/10.1029/2011GL050502

Tessier, B., Poirier, C., Weill, P., Dezileau, L., Lieux, A., Mouazé, D., Fournier, J., Bonnot-Courtois, C., 2019. Evolution of a Shelly Beach Ridge System over the Last Decades in a Hypertidal Open-coast Embayment (Western Mont-Saint-Michel Bay, NW France). J. Coast. Res. 88, 77–88. https://doi.org/10.2112/SI88-007.1

Thieler, E.R., Himmelstoss, E.A., Zichichi, J.L., Ergul, A., 2009. The Digital Shoreline Analysis System (DSAS) Version 4.0 - An ArcGIS extension for calculating shoreline change, Open-File Report. Reston, VA. https://doi.org/10.3133/ofr20081278

Time Series Analysis for Cyclostratigraphy, 2014. , in: Rock Magnetic Cyclostratigraphy. John Wiley & Sons, Ltd, pp. 52–89. https://doi.org/https://doi.org/10.1002/9781118561294.ch4

Vacchi, M., Engelhart, S.E., Nikitina, D., Ashe, E.L., Peltier, W.R., Roy, K., Kopp, R.E., Horton, B.P., 2018. Postglacial relative sea-level histories along the eastern Canadian coastline. Quat. Sci. Rev. 201, 124–146. https://doi.org/10.1016/j.quascirev.2018.09.043

Walters, D., Moore, L.J., Duran Vinent, O., Fagherazzi, S., Mariotti, G., 2014. Interactions between barrier islands and backbarrier marshes affect island system response to sea level rise: Insights from a coupled model. J. Geophys. Res. Earth Surf. 119, 2013–2031. https://doi.org/https://doi.org/10.1002/2014JF003091

Wang, J., Yang, B., Ljungqvist, F.C., Luterbacher, J., Osborn, T.J., Briffa, K.R., Zorita, E., 2017. Internal and external forcing of multidecadal Atlantic climate variability over the past 1,200 years. Nat. Geosci. 10, 512–517. https://doi.org/10.1038/ngeo2962

Wiberg, P.L., Fagherazzi, S., Kirwan, M.L., 2020. Improving Predictions of Salt Marsh

Evolution Through Better Integration of Data and Models. Ann. Rev. Mar. Sci. 12, 389–413. https://doi.org/10.1146/annurev-marine-010419-010610

Williams, H.F.L., 2013. 600-year sedimentary archive of hurricane strikes in a prograding beach ridge plain, southwestern Louisiana. Mar. Geol. 336, 170–183. https://doi.org/10.1016/j.margeo.2012.12.005

Williams, H.F.L., 2012. Magnitude of Hurricane Ike storm surge sedimentation: Implications for coastal marsh aggradation. Earth Surf. Process. Landforms 37, 901–906. https://doi.org/10.1002/esp.3252

Woodworth, P.L., 1999. High waters at Liverpool since 1768: The UK's longest sea level record. Geophys. Res. Lett. 26, 1589–1592. https://doi.org/10.1029/1999GL900323

Woodworth, P.L., Morales Maqueda, M., Gehrels, W.R., Roussenov, V.M., Williams, R.G., Hughes, C.W., 2017. Variations in the difference between mean sea level measured either side of Cape Hatteras and their relation to the North Atlantic Oscillation. Clim. Dyn. 49, 2451–2469. https://doi.org/10.1007/s00382-016-3464-1

# Importance of coarse sediment deposition in the adaptation of back-barrier saltmarshes to sea-level rise

Goslin, J. [1,2], Bernatchez, P. [1], Barnett, R.L. [1,3], Ghaleb, B. [4], Béland, C. [1], Didier, D. [1], Garneau, M. [4]

## FIGURES

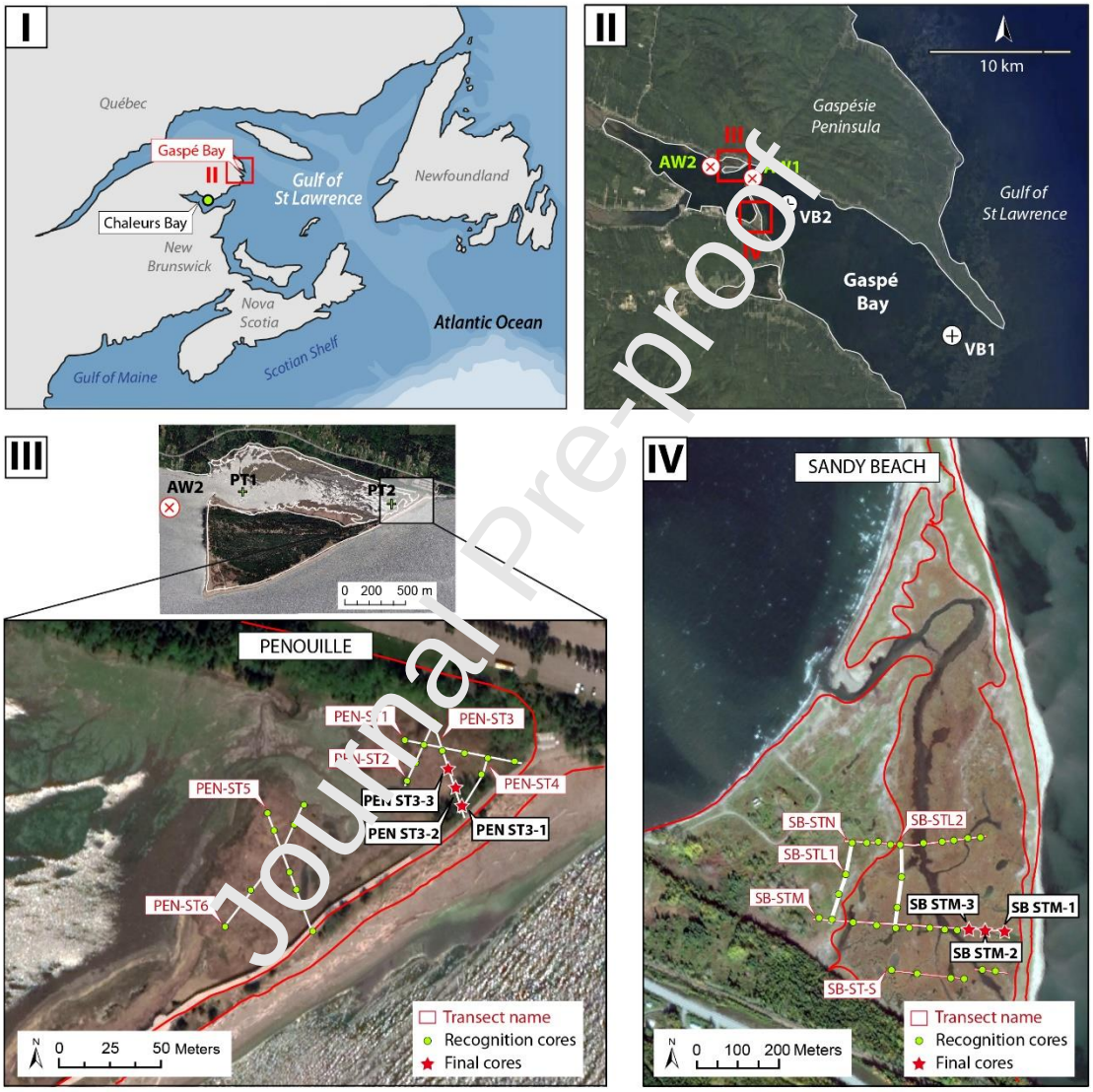


Figure 1. Maps showing the location of the study region (I) and study sites (II), as well as the location of the cores used in this study (III and IV). Black crossed-circles on (II) show the locations of Wave Watch III grid points used to derive local hydrodynamic conditions (section 3.2). Red crossed-circles on (II) and (III) show the locations AWAC measurements of Bernatchez et al. (2013), while green crosses noted PT1 and PT2 show the location of RBR measurements of Bernatchez et al. (2013) discussed in section 6.1.2.

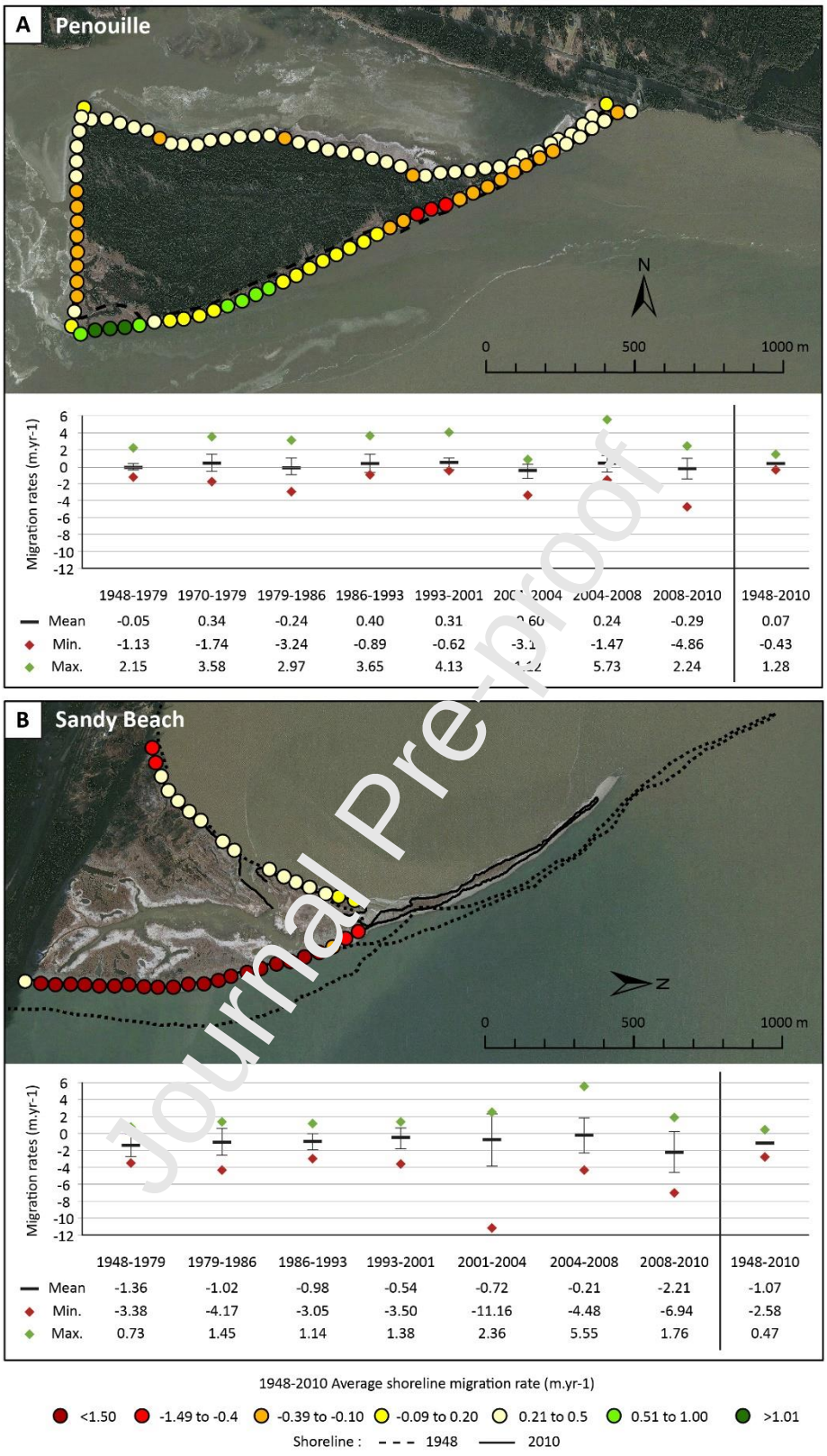


Figure 2. Shoreline migration rates for Penouille and Sandy Beach spits over the 1948-2010 period

(Data from Bernatchez et al., 2013)

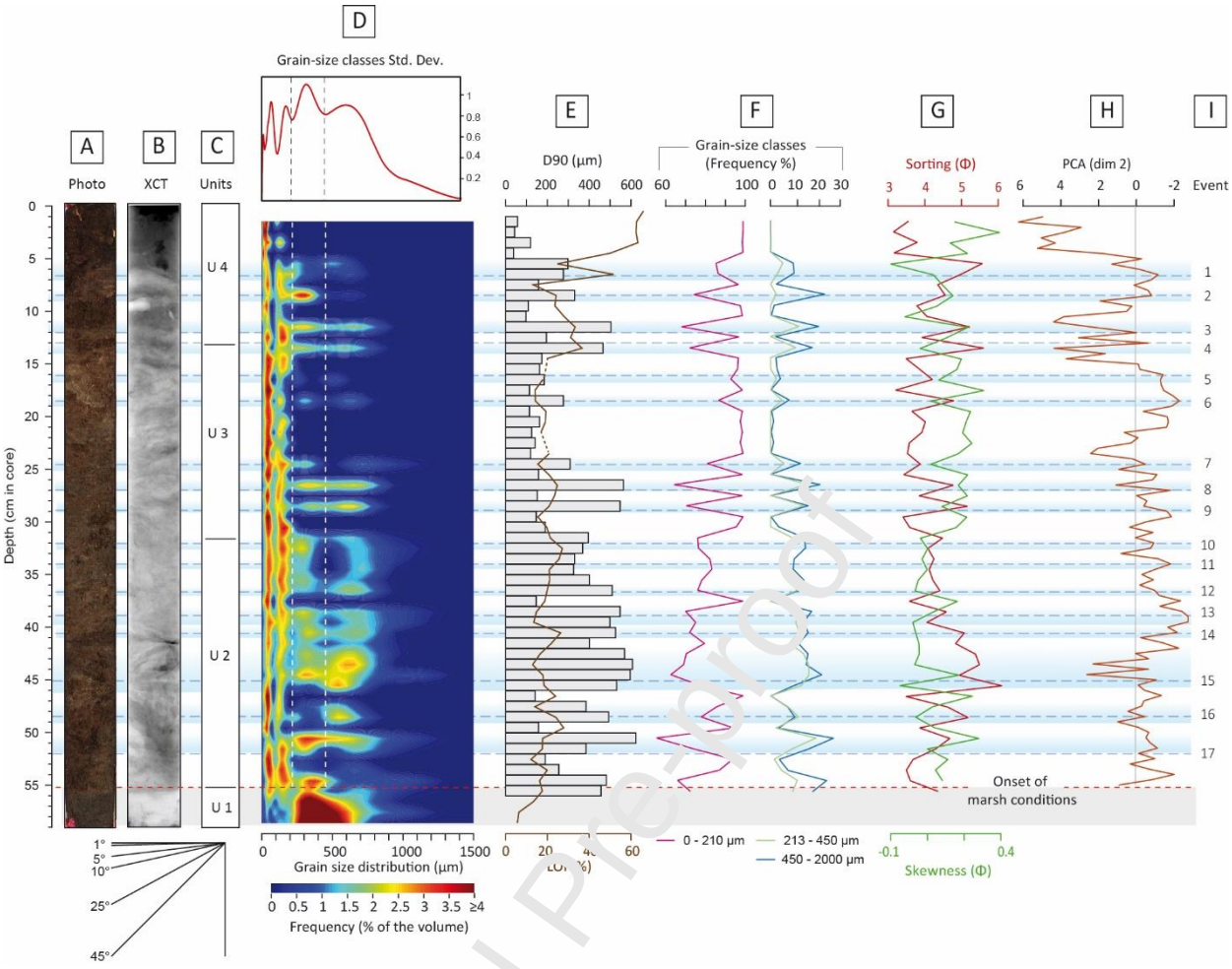


**Figure 3. (A)** Photography of core PEN-ST3-1, (B) XCT X-Ray image of core PEN-ST3-1, **(C)** Interpretative sedimentary units, **(D)** Grain-size distribution in frequency and intra-class standard deviation for each grain-size fraction (upper plot), **(E)** $D_{90}$ Grain size and Loss-On-Ignition plots, **(F)** Frequency of the 0-210 µm, 213-450 µm and 450-2000 µm grain-size classes, **(G)** Sorting and skewness index plots, **(H)** Down-core coordinates along dimension 2 of the PCA performed on major and trace geochemical elements (see Fig. 5-H). Horizontal blue bands show the stratigraphic position of the coarse-sedimentary events. The grey band at the bottom corresponds to the underlying deltaic sand deposit that was excluded from the analyses.

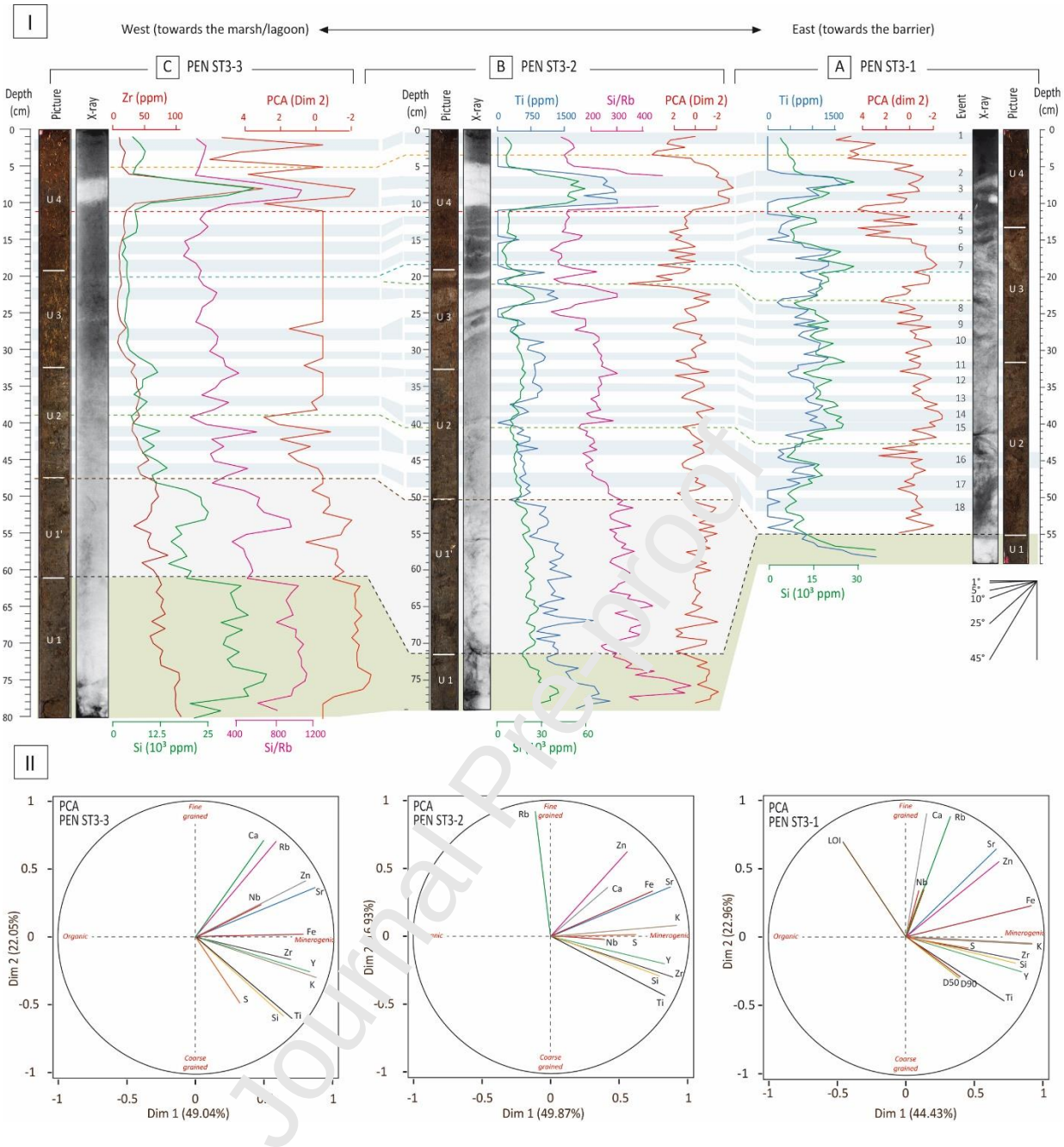


**Figure 4. (I)** Stratigraphic correlations between seaward core (A) PEN-ST3-1 and landwards cores (B) PEN-ST3-2 and (C) PEN-ST3-3. For each core are displayed the picture of the core along with interpretative sedimentary units, an XCT X-Ray image and plots of geochemical measurements: (i) Red solid lines show the downcore coordinates of PCA dimension 2 for each core. Negative excursions of PCA dim. 2 show the presence of coarser minerogenic material (note that the x-scale is inversed for this plot, so negative to the right). (ii) Blue and green solid line are for Ti and Si contents (in ppm), respectively. (iii) Dark red solid line on (C) show the downcore content in Zr instead of Ti for this core (faulty Ti data for this core). (iv) Pink solid line on (B) and (C) show the downcore variations of the Si/Rb ratio, used as a proxy of grain-size for these cores (see PCA loading plots below in II). (v) Horizontal blue shapes show tentative correlations between cores. (vi) Grey shape displays the position of unit U1', absent of core PEN-ST3-1. (vii) Brown shape shows the basal sand unit. **(II)** PCA loading plots of the sedimentological (LOI, D50, D90) and geochemical variables provided by the PCA performed on core PEN-ST3-1, 3-2 and 3-3 data (from right to left, respectively).

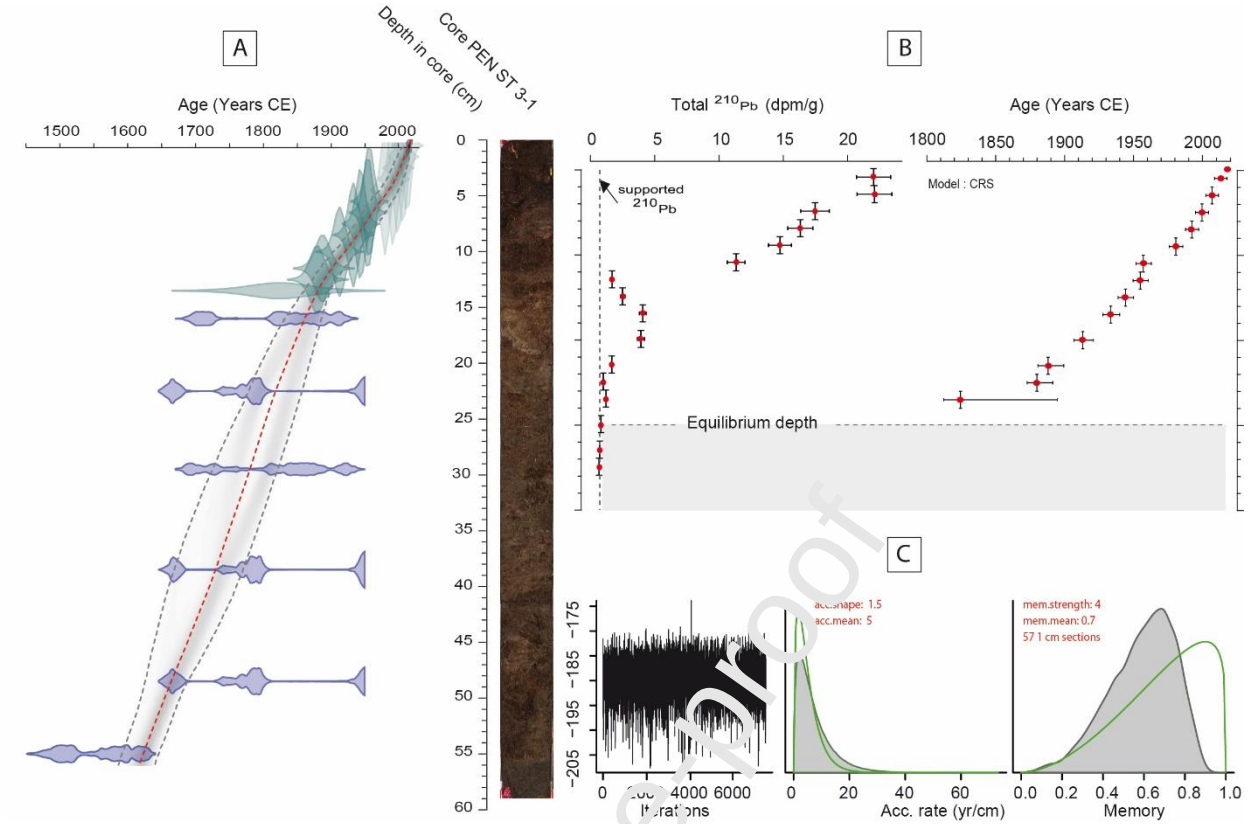


**Figure 5. (A)** Age model obtained for core PEN-ST3-1 based on the Bayesian analysis of $^{14}C$ (blue shapes) and $^{210}Pb$ ages (green shapes). Blue and green shapes show the probability distribution for each dated horizon. Grey envelope shows the 95% significance envelope. Red dotted line is the median age produced by the analysis. **(B)** $^{210}Pb$ measurements and $^{210}Pb$ based age-model (in years C.E.). **(C)** Parameters and outputs of the Bayesian calculation operated by the Bacon age-modelling software package.

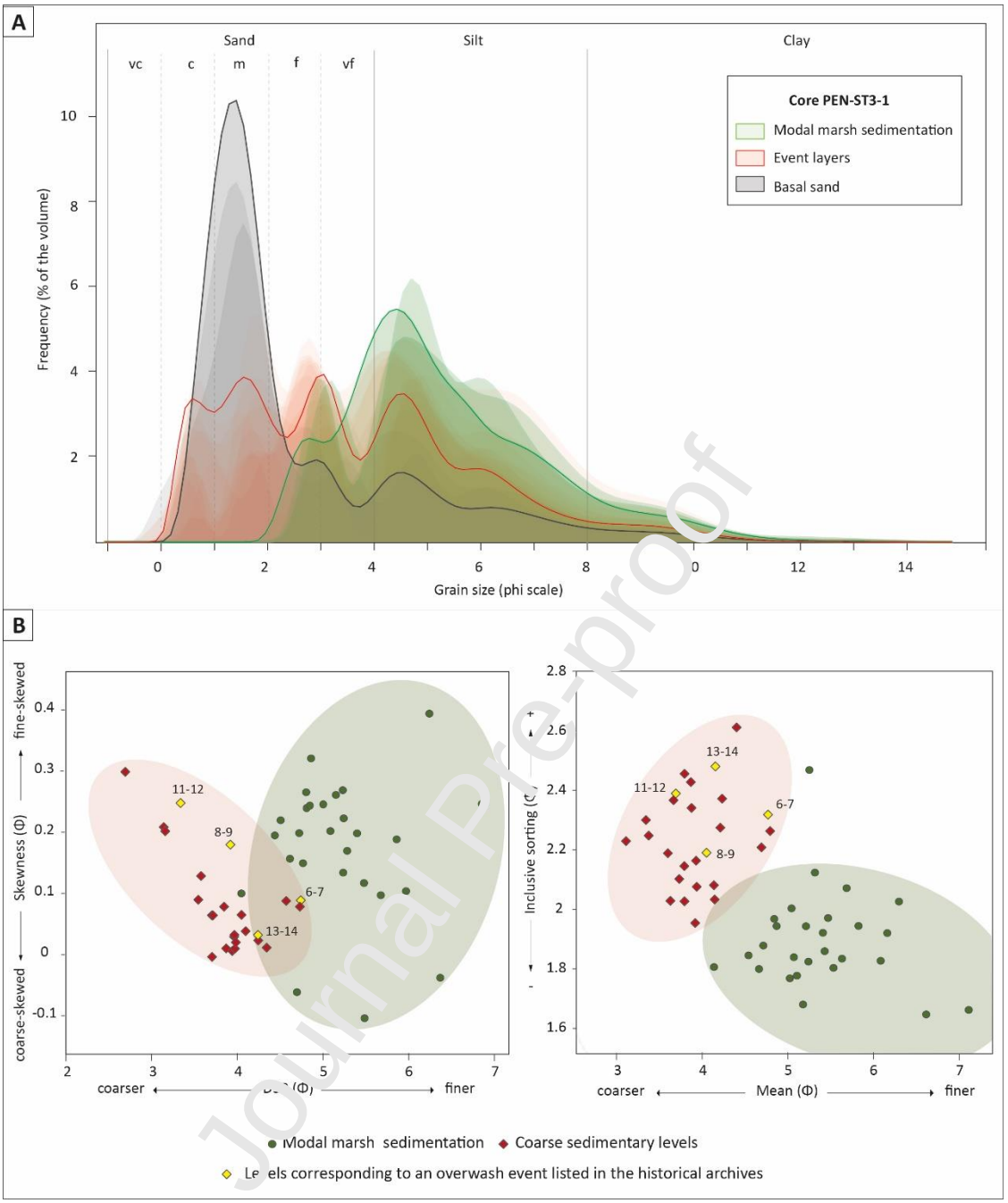


**Figure 6. (A)** Core PEN-ST3-1 grain-size frequency distribution of modal marsh fine grain sediments (green envelopes), coarse sedimentary layers (red envelopes) and basal sand unit (dark grey envelopes), **(B)** (LEFT) Skewness (Φ) vs $D_{50}$ and (RIGHT) Inclusive sorting vs Mean scatterplots for core PEN-ST3-1. Green dots are for levels of modal marsh sedimentation. Red diamonds stand for coarse sedimentary levels. The yellow diamonds show the position of the layers for which a correspondence with storms listed in the historical archives and having caused washover deposition on the marsh is highly likely (numbers refer to the depth of these layers in core).

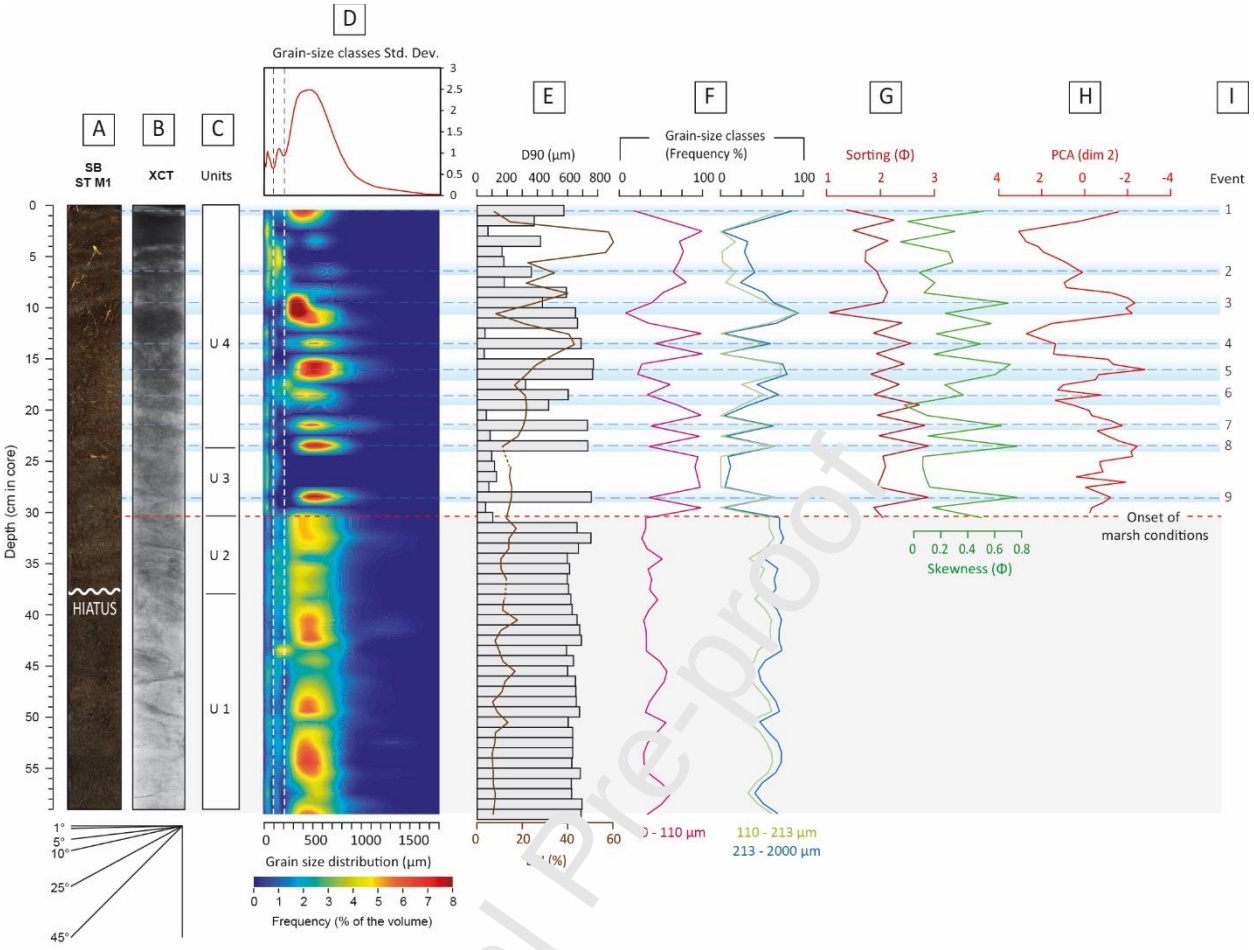


**Figure 7. (A)** Photography of core PEN-ST3-1, **(B)** XCT X-Ray image of core PEN-ST3-1, **(C)** Interpretative sedimentary units, **(D)** Grain-size distribution in frequency and inter-class standard deviation for each grain-size fraction (upper plot), **(E)** $D_{90}$ Grain size and Loss-On-Ignition plots, **(F)** frequency of the 0-110 µm, 110-213 µm and 213-2000 µm grain-size classes, **(G)** Sorting and skewness index plots, **(H)** Downcore coordinates along dimension 2 of the PCA performed on major and trace geochemical elements (see Fig. 9 II). Horizontal blue bands show the stratigraphic position of the coarse-sedimentary events here interpreted to originate from overwash submersive events. The grey band at the bottom corresponds to sandflat coarse deposits from which abnormally coarse sedimentary events could not be deciphered.

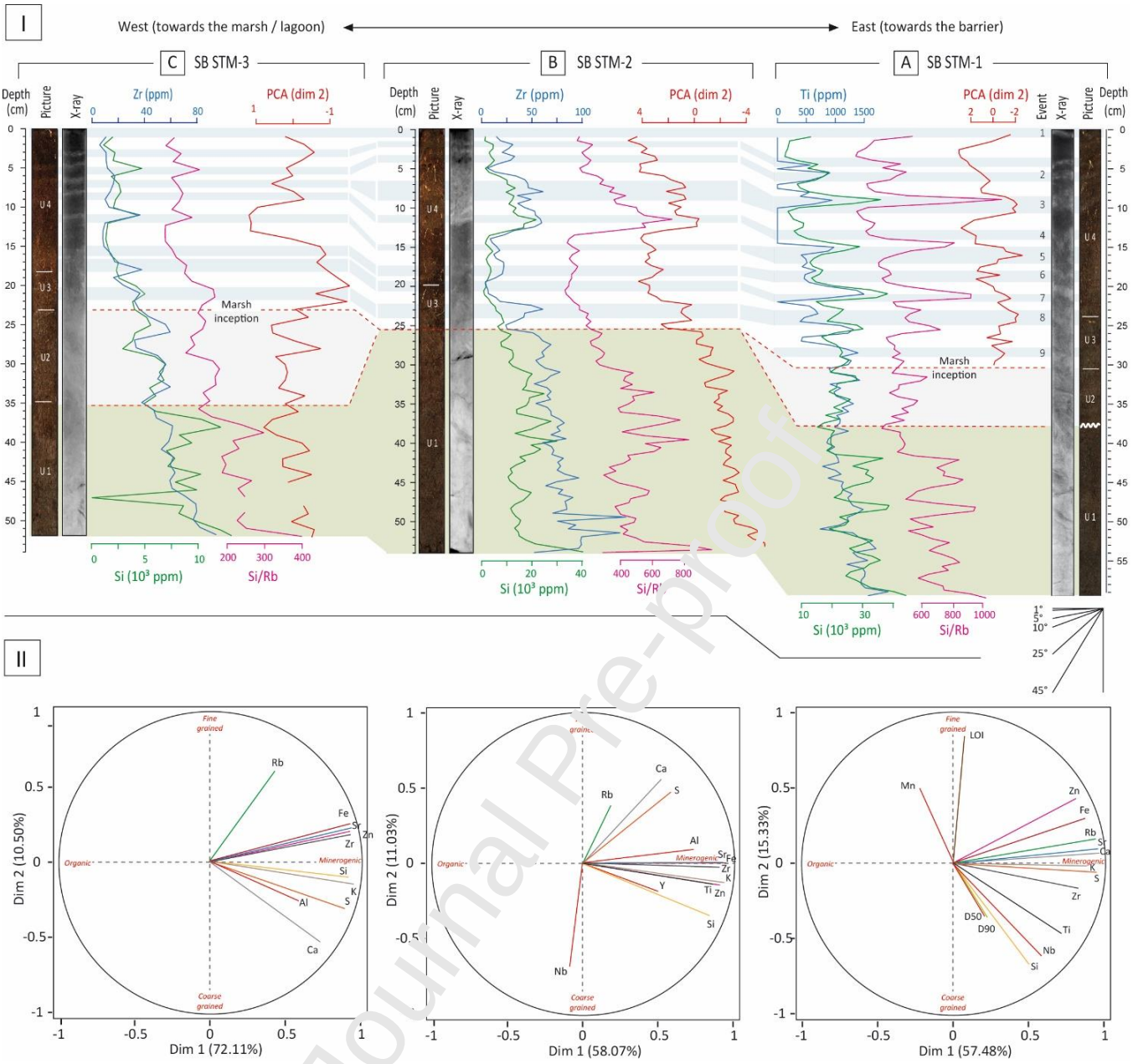


**Figure 8. (I)** Stratigraphic correlations between seaward core (A) SB-STM-1 and landwards cores (B) SB-STM-2 and (C) SB-STM-3. For each core are displayed the picture of the core along with interpretative sedimentary units, an XCT X-Ray image and plots of geochemical measurements: (i) Red solid lines show the downcore coordinates of PCA dimension 2 for each core. Negative excursions of PCA dim. 2 show the presence of coarser minerogenic material (note that the x-scale is inversed for this plot, so negative to the right). (ii) Blue and green solid line on A are for Ti and Si contents (in ppm), respectively. (iii) Blue solid line on (B) and (C) show the contents in Zr instead of Ti for these cores. (iv) Pink solid line on (B) and (C) show the downcore variations of the Si/Rb ratio, used as a proxy of grain-size for these cores (see PCA loading plots below in II). (v) Horizontal blue shapes show tentative correlations between cores. (vi) Grey shape displays the position of unit U2, not found in core SB-STM-2. (vii) Brown shape shows the basal sand unit. **(II)** PCA loading plots of the sedimentological (LOI, D50, D90) and geochemical variables provided by the PCA performed on core SB-STM-1, STM-2 and STM-3 data (from right to left, respectively).

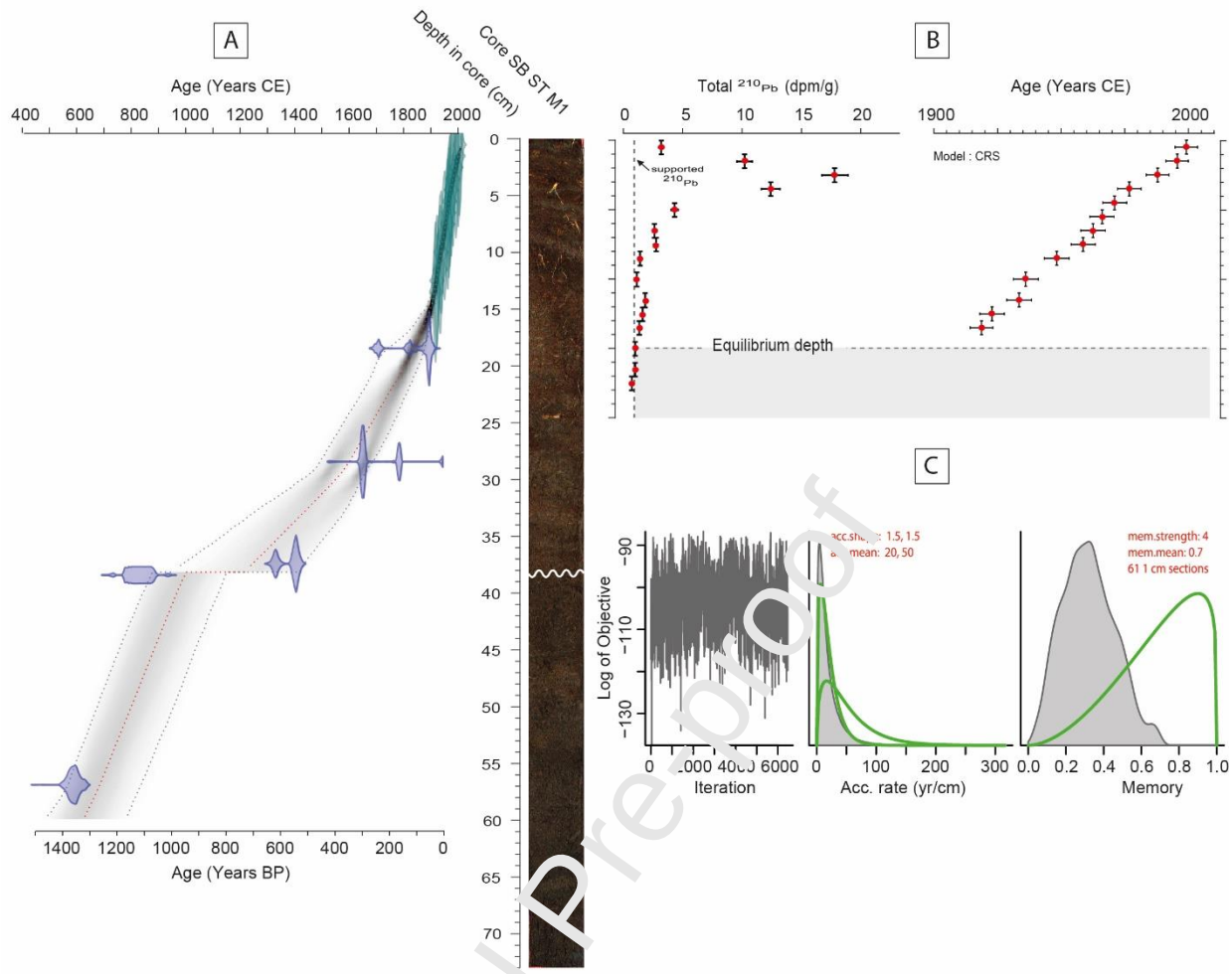


**Figure 9. (A)** Age model obtained for core SB-ST M1 based on the Bayesian analysis of $^{14}C$ (blue shapes) and $^{210}Pb$ ages (green shapes). Blue and green shapes show the probability distribution for each dated horizon. Grey envelope shows the 95% significance envelope. Red dotted line is the median age produced by the analysis. **(B)** $^{210}Pb$ measurements and $^{210}Pb$ based age-model (in years C.E.). **(C)** Parameters and outputs of the Bayesian calculation operated by the Bacon age-modelling software package.

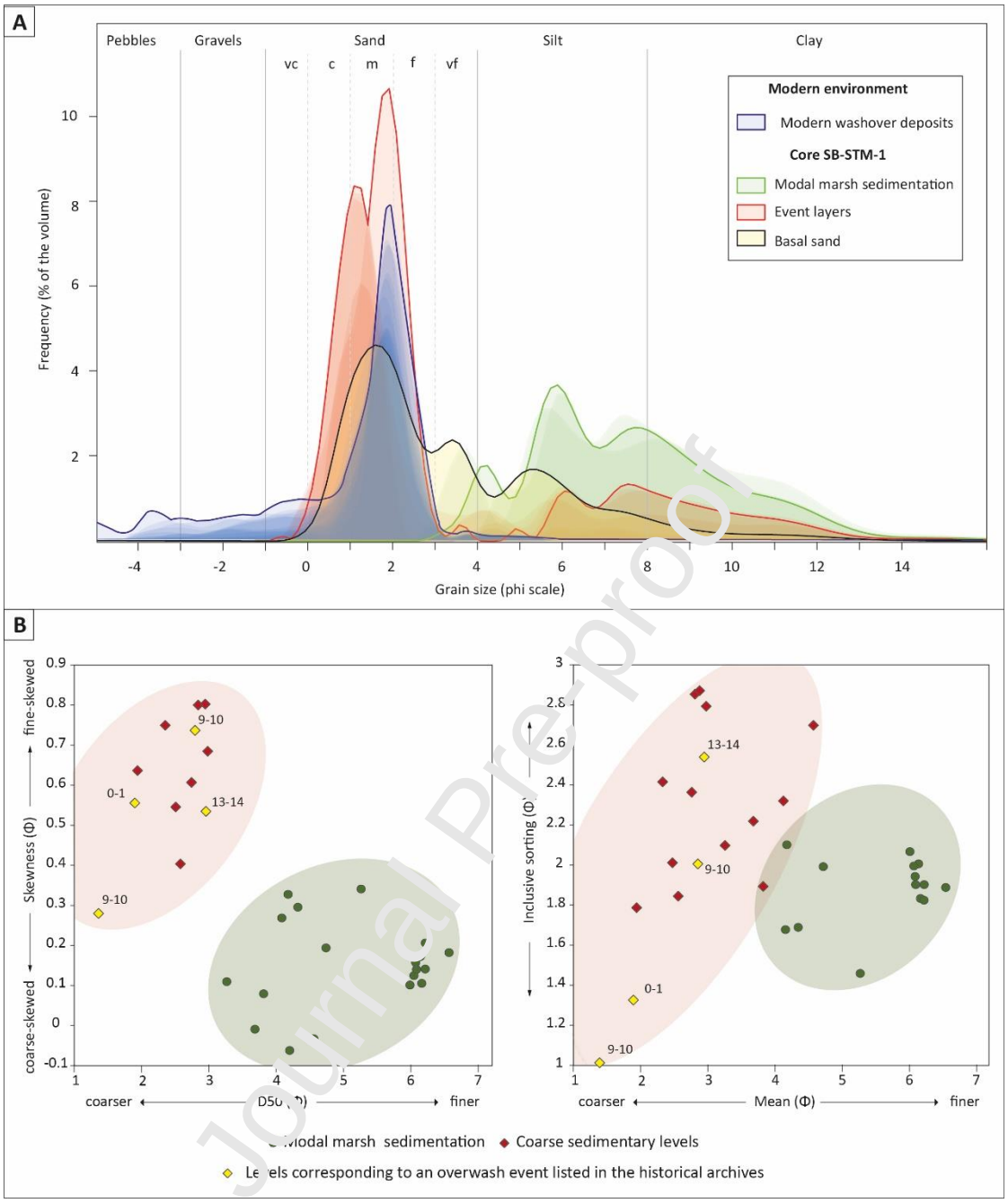


**Figure 10. (A)** Grain-size frequency distribution of modern washover deposits (blue envelope) and of core SB-STM-1 modal marsh fine grain sediments (green envelopes), coarse sedimentary layers (red envelopes) and basal sand unit (dark grey envelopes), **(B)** (LEFT) Skewness (Φ) vs $D_{50}$ and (RIGHT) Inclusive sorting vs Mean scatterplots for core PEN-ST3-1. Green dots are for levels of modal marsh sedimentation. Red diamonds stand for coarse sedimentary levels. The yellow diamonds show the position of the layers for which a correspondence with storms listed in the historical archives and having caused overwash deposition on the marsh is highly likely (numbers refer to the depth of these layers in core).

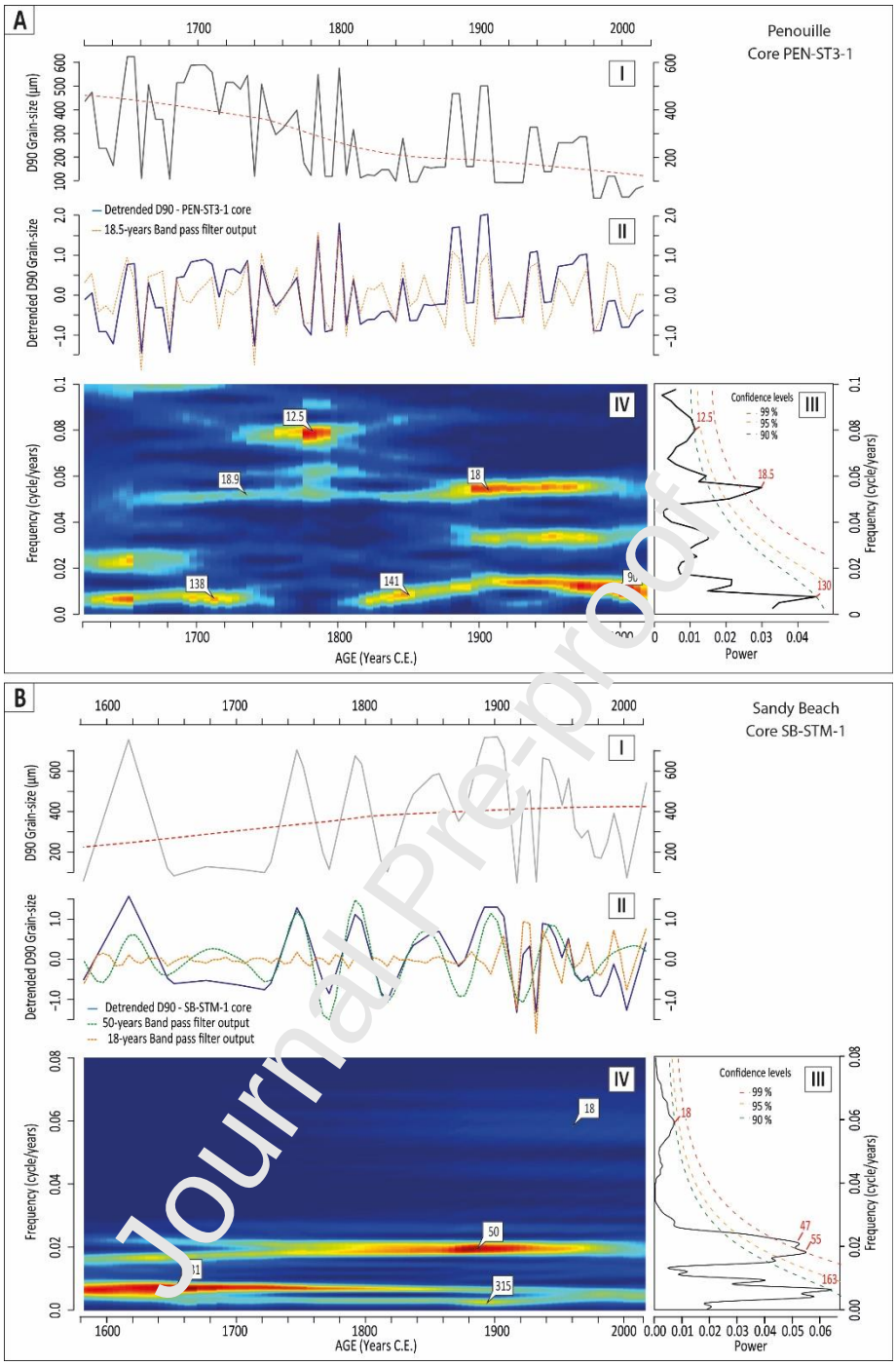


**Figure 11.** Results of the spectral analyses (Multi Taper Spectrum, MTM) and Evolutive Harmonic Analyses (EHA) performed **(A)** on the PEN-ST3-1 $D_{90}$ grain-size time-series for the 1620-2018 C.E. period and **(B)** on the SB-STM-1 $D_{90}$ grain-size time-series for the 1580-2018 C.E. period. For both figures: **(I)** Raw time-series (Black curve), LOWESS smoothing (dotted red curve) **(II)** ***(Blue curve)*** $D_{90}$ grain size time-series detrended from long-term tendency using results of the band-pass filters applied to the grain-size time-series (dotted red curve on I), ***(Yellow curve)*** Output of the 18-yrs bandpass filter, ***(Green curve)*** Output of the 50-yrs bandpass filter. **(III)** Frequency power spectra of the $D_{90}$ grain-size time-series. Red numbers indicate the main periodicities present in the record, **(IV)** Evolutive Harmonic Analysis diagram, showing the evolution of the periodicities with time. The blue to red color scale on indicates the power of the frequencies (Blue-low power, Red-high power) and their evolution through time (in years C.E.). The white numbers on the EHA diagrams are reading guides that help to locate and follow the evolution with time of the dominant periodicities shown on diagram III.




**Figure 12. (I)** Pictures of different areas of the Penouille Spit. Location of the pictures are shown on the aerial photograph, along with the direction in which they were taken. **(A and B)** Storm deposits over the east isthmus, December 2010 (Copyright Parcs Canada), **(C)** Active micro-cliff at the distal end section of Penouille spit, near the entrance of the lagoon. **(D)** Small lagoonal internal sand-spits (extending towards the east), **(E)** Sand beach established between the marsh and the inner part of the Penouille Spit, **(F)** Aerial view of the impacts of the storm of December 30, 2016 on the Penouille isthmus. Red line marks the high-water line of wooden debris and trunk deposited on the inner lagoonal side of the back-barrier marsh. **(II)** (A) Aerial image of Sandy Beach site and **(B)** Oblique images from 2010 (B-I) and 2017 (B-II) showing the extension of washovers blankets induced by the storm of December 30, 2016 on the site (eye on the aerial photograph shows the location and framing of the oblique images).

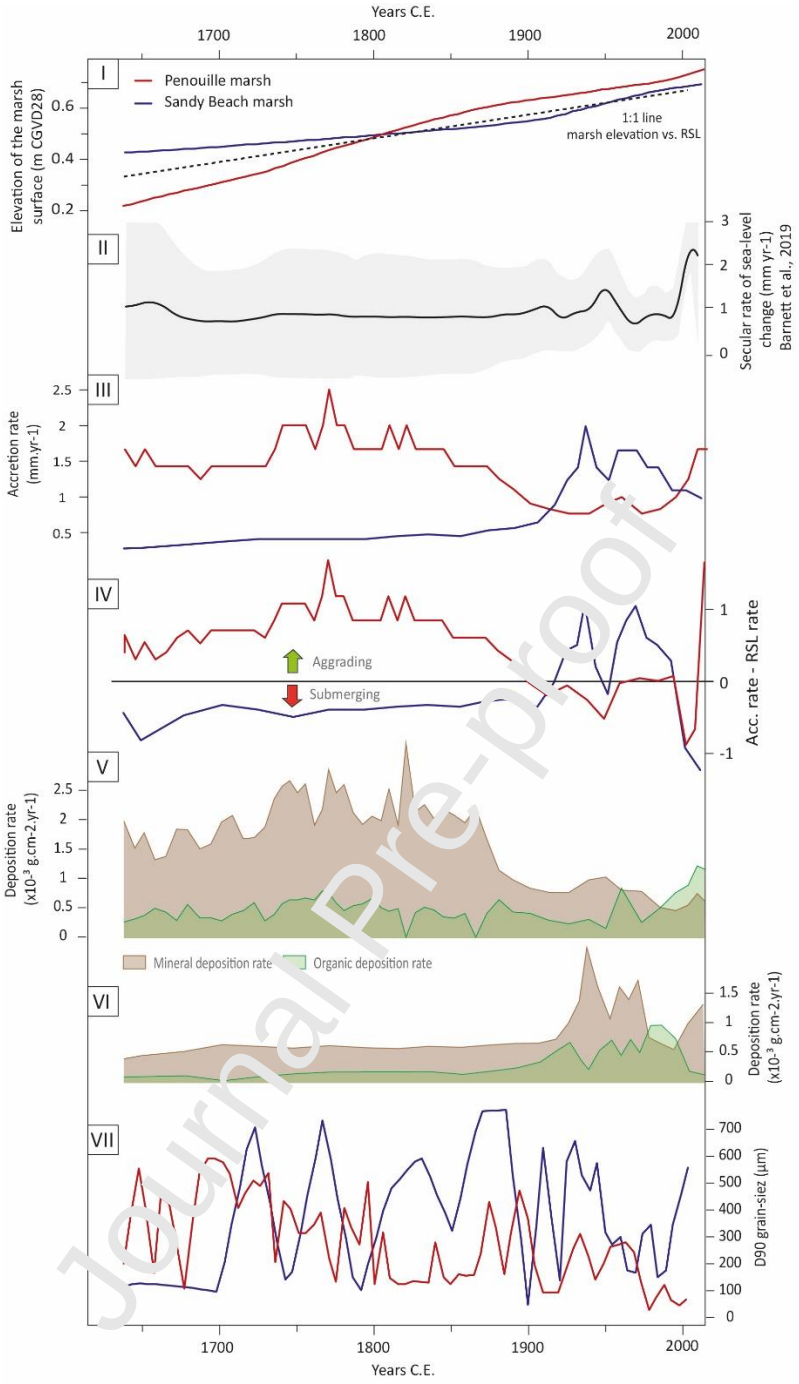


**Figure 13. (I)** Evolution of the Penouille and Sandy Beach marshes surfaces as a function of mean relative sea level rise slope (data of Barnett *et al.*, 2019, simplified by linear regression. Note that the dotted line shows RSL rise slope, not RSL elevation). **(II)** Secular rates of relative sea-level change (data from nearby Baie-des-Chaleurs, Barnett et al., 2019). **(III)** Accretion rates at the surface of Penouille and Sandy beach marshes. **(IV)** Accretion rate minus RSL diagram. Negative values indicate submergence of the marshes, positive values show aggradation of the marshes at the location of studied cores. **(V)** Temporal evolution of the minerogenic and organogenic deposition rates at the surface of Penouille marsh, **(VI)** Temporal evolution of the **m**inerogenic and organogenic deposition rates at the surface of Sandy Beach marsh. **(VII)** D90 grain-size time-series for both marshes, used as a record of coarse minerogenic deposition upon the marshes.

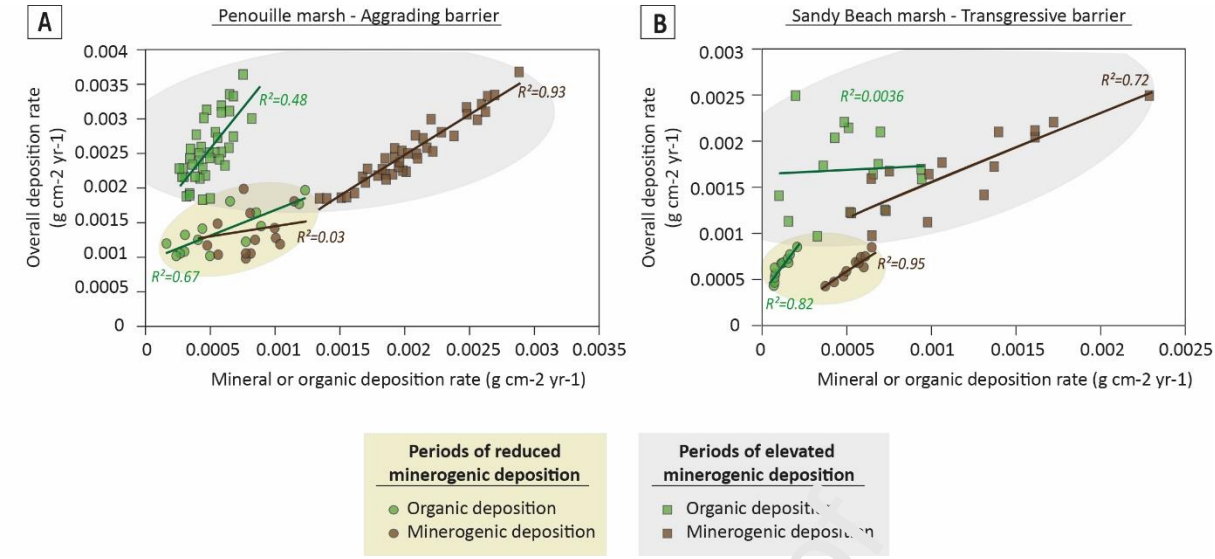


**Figure 14.** Scatterplots of Overall deposition rates as a function of mineral (brown symbols) and organogenic (green symbols) deposition rates at the surface of (A) Penouille and (B) Sandy Beach marshes, during periods of elevated and reduced minerogenic deposition.

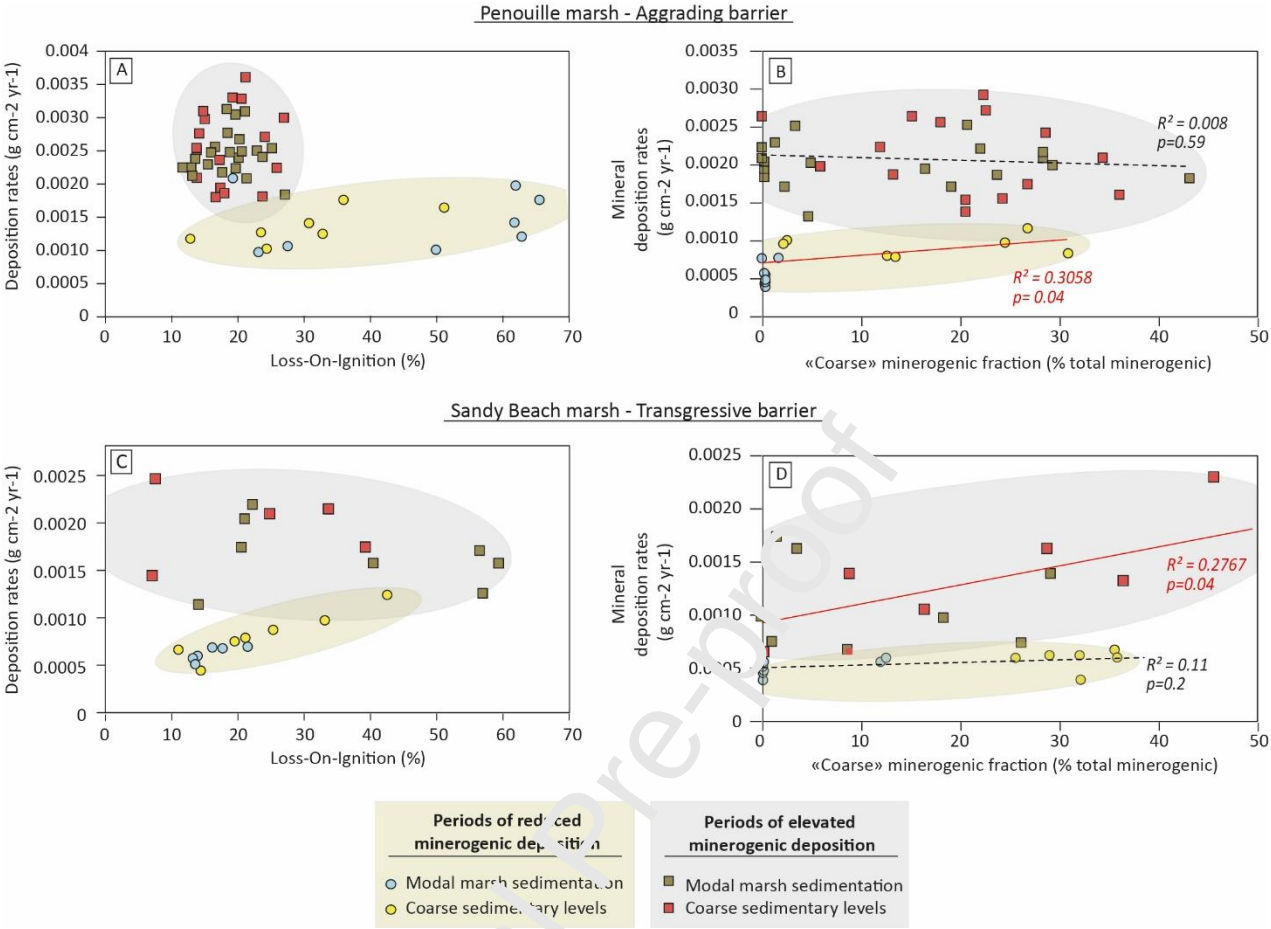


**Figure 15. (A and C)** Scatterplots of deposition rates vs. loss on ignition values and **(B and D)** Scatterplots of mineral deposition rates vs. Percentage of "coarse" minerogenic fraction in the total minerogenic component during periods of reduced minerogenic deposition (brown shapes) and elevated minerogenic deposition (green shapes) at the surface of Penouille and Sandy Beach marshes.

| Univ. of California # | Univ. Laval # | Core | Depth (cm) | Material | $D^{14}C$ (‰) | ± | $^{14}C$ age (conv. BP) | ± | Age (cal. BP) max (med) min IntCal 13 |
|---|---|---|---|---|---|---|---|---|---|
| UCIAMS-224493 | ULA-8745 | PEN ST 3-1 | 15-17 | Alnus sp. & Betula sp. seeds | -12.12 | 2.0 | 100 | 20 | 255 (**115**) 30 |
| UCIAMS-225987 | ULA-8746 | PEN ST 3-1 | 22-23 | Alnus sp. & Betula sp. seeds | -25.5 | 2.2 | 205 | 20 | 295 (**170**) 0 |
| UCIAMS-225986 | ULA-8744 | PEN ST 3-1 | 29-30 | Abies balsamea needle | -15.3 | 2.2 | 125 | 20 | 265 (**106**) 15 |
| UCIAMS-213444 | ULA-8295 | PEN ST 3-1 | 38-39 | Alnus sp. seeds | -24.7 | 1.7 | 200 | 15 | 290 (**168**) 0 |
| UCIAMS-213442 | ULA-8293 | PEN ST 3-1 | 48-49 | Alnus sp. & Betula sp. seeds | -25.1 | 1.8 | 205 | 20 | 295 (**180**) 0 |
| UCIAMS-213443 | ULA-8294 | PEN ST 3-1 | 55.5-56. 5 | Alnus sp. seeds | -41.8 | 1.7 | 345 | 15 | 478 (**381**) 317 |
| UCIAMS-215556 | ULA-8371 | SB-ST M1 | 18-19 | Salt-marsh plants rhizomes | -0.2 | 1.8 | 0 | 15 | **Modern** |
| UCIAMS-215548 | ULA-8370 | SB-ST M1 | 28-29 | Salt-marsh plants rhizomes | -29.7 | 1.7 | 240 | 15 | 300 (**292**) 160 |
| UCIAMS-225989 | ULA-8748 | SB-ST M1 | 36-37 | Salt-marsh plants rhizomes | -25.5 | 2 | 545 | 20 | 625 (**545**) 525 |
| UCIAMS-225988 | ULA-8747 | SB-ST M1 | 37-38 | Wood fragment | -138 | 2.1 | 1195 | 20 | 1175 (**1112**) 1070 |
| UCIAMS-213445 | ULA-8296 | SB-ST M1 | 56-58 | Cyperaceous fragments | -167.7 | 1.5 | 1475 | 15 | 1390 (**1360**) 1320 |

Table 1. $^{14}C$ AMS radiocarbon dating performed on cores PEN-ST3-1 and SB-STM-1

| Lab. Code UQPo | Sample ID | Mean depth | $^{210}$Pb dpm/g | ± | Mean age | Min. age | Max. age | Mean date | Min. date | Max. date |
|---|---|---|---|---|---|---|---|---|---|---|
| **PENOUILLE – Core PEN-ST3-1** | | | | | | | | | | |
| | Surface | **0** | n/a | n/a | 0 | 0 | 0 | **2018** | 2018 | 2018 |
| 9733 | PEN 0-1 | **0.5** | 21.995 | 1.331 | 5.2 | 0.7 | 9.8 | **2013** | 2017 | 2008 |
| 9734 | PEN 1-2 | **1.5** | 22.078 | 1.346 | 11.5 | 6.9 | 16.2 | **2006** | 2011 | 2002 |
| 9585 | PEN 2-3 | **2.5** | 17.441 | 1.109 | 18.8 | 14.2 | 23.5 | **1999** | 2004 | 1994 |
| 9735 | PEN 3-4 | **3.5** | 16.292 | 0.988 | 26.1 | 21.4 | 30.9 | **1992** | 1997 | 1987 |
| 9736 | PEN 4-5 | **4.5** | 14.709 | 0.893 | 37.8 | 32.9 | 42.8 | **1980** | 1985 | 1975 |
| 9737 | PEN 5-6 | **5.5** | 11.296 | 0.692 | 61.4 | 56.0 | 67.1 | **1957** | 1962 | 1951 |
| 9738 | PEN 6-7 | **6.5** | 1.630 | 0.107 | 63.6 | 58.2 | 69.3 | **1954** | 1960 | 1949 |
| 9587 | PEN 7-8 | **7.5** | 2.451 | 0.179 | 74.3 | 68.9 | 80.3 | **1944** | 1949 | 1938 |
| 9739 | PEN 8-9 | **8.5** | 4.026 | 0.253 | 85.0 | 79.4 | 91.5 | **1933** | 1939 | 1927 |
| 9588 | PEN 9.5-10.5 | **10** | 3.880 | 0.269 | 105.3 | 97.1 | 113.2 | **1913** | 1919 | 1905 |
| 9740 | PEN 11-12 | **11.5** | 1.607 | 0.108 | 130.4 | 122.9 | 141.7 | **1888** | 1895 | 1876 |
| 9589 | PEN-12-13 | **12.5** | 0.954 | 0.086 | 138.6 | 131.5 | 150.1 | **1879** | 1886 | 1868 |
| 9741 | PEN 13-14 | **13.5** | 1.157 | 0.08[illegible] | 193.9 | 181.7 | 264.0 | **1824** | 1836 | 1754 |
| 9560 | PEN 14.5-15.5 | **15** | 0.765 | 0.07[illegible] | n/a | n/a | n/a | **n/a** | n/a | n/a |
| 9742 | PEN 16-17 | **16.5** | 0.679 | 0.049 | n/a | n/a | n/a | **n/a** | n/a | n/a |
| 9743 | PEN 17-18 | **17.5** | 0.621 | 0.045 | n/a | n/a | n/a | **n/a** | n/a | n/a |
| **SANDY BEACH – Core SB-STM-1** | | | | | | | | | | |
| | Surface | **0** | 0.000 | 0.000 | 0 | 0 | 0 | **2018** | 2018 | 2018 |
| 9755 | SB 0-1 | **0.5** | 3.154 | 0.201 | 10.0 | 5.3 | 14.7 | **2008** | 2013 | 2003 |
| 9756 | SB 1-2 | **1.5** | 10.173 | 0.636 | 13.9 | 9.2 | 18.7 | **2004** | 2009 | 1999 |
| 9757 | SB 2-3 | **2.5** | 17.775 | 1.101 | 22.3 | 17.4 | 27.2 | **1996** | 2001 | 1991 |
| 9758 | SB 3-4 | **3.5** | 12.345 | 0.773 | 34.6 | 29.5 | 39.6 | **1983** | 1988 | 1978 |
| 9759 | SB 4.5-5.5 | **5** | 4.302 | 0.279 | 40.8 | 35.8 | 46.0 | **1977** | 1982 | 1972 |
| 9760 | SB 6-7 | **6.5** | 2.588 | 0.172 | 46.2 | 41.1 | 51.4 | **1972** | 1977 | 1967 |
| 9761 | SB 7-8 | **7.5** | 2.686 | 0.177 | 50.1 | 45.0 | 55.4 | **1968** | 1973 | 1963 |
| 9762 | SB 8-9 | **8.5** | 1.394 | 0.097 | 54.3 | 49.2 | 59.5 | **1964** | 1969 | 1958 |
| 8763 | SB 9.5-10.5 | **10** | 1.112 | 0.082 | 65.6 | 60.4 | 70.8 | **1952** | 1958 | 1947 |
| 9764 | SB 11-12 | **11.5** | 1.822 | 0.127 | 78.8 | 73.5 | 84.3 | **1939** | 1944 | 1934 |
| 9765 | SB 12-13 | **12.5** | 1.556 | 0.111 | 81.7 | 76.5 | 87.0 | **1936** | 1941 | 1931 |
| 9766 | SB 13-14 | **13.5** | 1.315 | 0.093 | 93.3 | 88.2 | 98.6 | **1925** | 1930 | 1919 |

| | | | | | | | | | | |
|---|---|---|---|---|---|---|---|---|---|---|
| 9767 | SB 14.5-15.5 | **15** | 0.906 | 0.061 | 97.8 | 92.9 | 102.7 | **1920** | 1925 | 1915 |
| 9768 | SB 16-17 | **16.5** | 0.958 | 0.066 | n/a | n/a | n/a | **n/a** | n/a | n/a |
| 9769 | SB 17-18 | **17.5** | 0.641 | 0.045 | n/a | n/a | n/a | **n/a** | n/a | n/a |

Table 2. Ages obtained for cores PEN-ST3-1 and SB-STM-1 from $^{210}$Pb radionuclide measurements.

| | Penouille | | Sandy Beach | |
|---|---|---|---|---|
| | Beach-spit system | Marsh | Beach-spit system | Marsh |
| Area (ha) 1948 | - | - | 37,714 | 33,631 |
| Area (ha) 1963 | 60,645 | 21,463 | - | - |
| Area (ha) 2008 | 62,769 | 21,180 | 16,848 | 25,454 |
| Variation of the area (ha) | +2,124 | -0,284 | -20,866 | -8,177 |
| % gain or loss over historical area | +3,50 % | -1,32 % | -55,33 % | -24,31 % |

**Table 3.** Evolution of the surface areas of the Penouille and Sandy Beach beach-spit and marsh systems.

| | PENOUILLE - Core PEN-ST3-1 | | | SANDY BEACH - Core SB-STM-1 | | |
|---|---|---|---|---|---|---|
| **Event** | **Depth (cm) Peak (range)** | **Age C.E. Max. (Med.) Min.** | | **Depth (cm) Peak (range)** | **Age C.E. Max. (Med.) Min.** | **Possible corresponding submersion events listed in the archives** (max. likelihood) |
| **-** | - | - | 1 | 0.5 (0-1) | 1990 (2012) 2018 | Oct. 15th 2003, Dec. 1-3rd 2005, Nov. 5th 2010, Dec. 6th 2010, Nov. 11th 2011, Dec. 30th 2016 |
| **1** | 6.5 (6-7.5) | 1937 (1960) 1986 | 2 | 6 (5.5-6.5) | 1954 (1967) 1978 | Dec. 6-11th 1950, Dec. 17-18th 1960, Nov. 20-28th 1968, Dec. 5th 1968 |
| **2** | 8.5 (8-9) | 1917 (1939) 1964 | 3 | 9.5 (8.5-10.5) | 1928 (1944) 1960 | Oct. 18-20th 1927, Dec. 6-11th 1950 |
| **3** | 12 (11-12) | 1877 (1901) 1927 | 4 | 13.5 (13-14) | 1897 (1917) 1931 | Oct. 20th 1913 |
| **4** | 13 (13-14) | 1853 (1881) 1903 | 5 | 16 (15-17) | 1801 (1883) 1916 | Nov. 5-7th 1884 |
| **5** | 16 (15.5-16.5) | 1827 (1862) 1888 | 6 | 18.5 (18-19.5) | 1704 (1835) 1885 | No archives |
| **6** | 18.5 (18-19) | 1804 (1845) 1877 | 7 | 21.5 (21-22) | 1652 (1771) 1838 | |
| **7** | 24.5 (24-25) | 1758 (1810) 1850 | 8 | 23.5 (23-24) | 1601 (1725) 1800 | |
| **8** | 27 (26-27) | 1743 (1799) 1840 | 9 | 28.5 (28-29) | 1473 (1582) 1699 | |
| **9** | 29 (28-29) | 1728 (1787) 1829 | | | | |
| **10** | 32 (31.5-32.5) | 1704 (1769) 1810 | | | | |
| **11** | 34 (33.5-34.5) | 1691 (1759) 1799 | | | | |
| **12** | 36.5 (36-37) | 1679 (1749) 1788 | | | | |
| **13** | 38.5 (38-39) | 1665 (1736) 1776 | | | | |
| **14** | 40.5 (40-41) | 1655 (1723) 1760 | | | | |
| **15** | 45 (42-46) | 1634 (1691) 1746 | | | | |
| **16** | 48.5 (47-49) | 1623 (1669) 170[illegible] | | | | |
| **17** | 52 (50-52) | 1614 (1649) 1670 | | | | |

**Table 4.** Depths and maximal, median and minimal ages of the coarse sedimentation events recorded in core PEN ST 3-1 (Penouille marsh) and in core SB ST M1 (Sandy Beach marsh). Rightmost column: Storm and submersion events listed in the archive known for having caused - or likely to have caused - washover deposition upon the marshes. Most likely events are underlined.

**Highlights**

- Last centuries records of coarse sedimentary deposition are reconstructed from two saltmarshes.
- Large-scale climate dynamics and the nodal tidal cycle control coarse minerogenic sedimentation.
- Periods of enhanced minerogenic deposition are driven by episodic coarse sediment inputs.
- Saltmarshes pseudo-equilibrium with RSL partly depends on episodic coarse inputs.
- Capacity of coarse sedimentary material to reach back-barrier marshes should be promoted.

Brest, December 8th 2021

As first author of the article entitled “Importance of coarse sedimentation for the resilience of back-barrier salt-marshes to sea-level rise”, submitted for publication in Marine Geology, I hereby declare that I, and all the listed co-authors, don’t have any conflict of interest to report concerning the way the data presented in this article was produced, nor concerning the writing of the articles and the results that are presented.

On behalf of all the co-authors

Jérôme Goslin

Coastal sedimentologist

IFREMER- Géosciences Marines

1625 Rte de St-Anne

29280 Plouzané

France